nature genetics

ARTICLES

https://doi.org/10.1038/s41588-021-00812-3

Ultraconserved enhancer function does not require perfect sequence conservation

Valentina Snetkova[1], Athena R. Ypsilanti[2], Jennifer A. Akiyama[1], Brandon J. Mannion[1,3], Ingrid Plajzer-Frick[1], Catherine S. Novak[1], Anne N. Harrington[1], Quan T. Pham[1], Momoe Kato[1], Yiwen Zhu[1], Janeth Godoy[1], Eman Meky[1], Riana D. Hunter[1], Marie Shi[1], Evgeny Z. Kvon[1,6], Veena Afzal[1], Stella Tran[1], John L. R. Rubenstein[2], Axel Visel[1,4,5]✉, Len A. Pennacchio[1,3,4]✉ and Diane E. Dickel[1]✉

Ultraconserved enhancer sequences show perfect conservation between human and rodent genomes, suggesting that their functions are highly sensitive to mutation. However, current models of enhancer function do not sufficiently explain this extreme evolutionary constraint. We subjected 23 ultraconserved enhancers to different levels of mutagenesis, collectively introducing 1,547 mutations, and examined their activities in transgenic mouse reporter assays. Overall, we find that the regulatory properties of ultraconserved enhancers are robust to mutation. Upon mutagenesis, nearly all (19/23, 83%) still functioned as enhancers at one developmental stage, as did most of those tested again later in development (5/9, 56%). Replacement of endogenous enhancers with mutated alleles in mice corroborated results of transgenic assays, including the functional resilience of ultraconserved enhancers to mutation. Our findings show that the currently known activities of ultraconserved enhancers do not necessarily require the perfect conservation observed in evolution and suggest that additional regulatory or other functions contribute to their sequence constraint.

Sequence conservation between species over long evolutionary times indicates purifying selection and is widely used to identify functional elements within genomes. Despite ~80 million years separating humans and rodents from their last common ancestor, 481 loci of at least 200 contiguous base pairs in the human genome were found to be perfectly identical to orthologous sequences in mice and rats[1]. These 'ultraconserved' human–rodent loci also show a high degree of conservation throughout an additional ~100 sequenced vertebrate genomes[2] (Fig. 1a). Ultraconserved sequences were initially shown to be depleted of common single-nucleotide polymorphisms in the human population[1,3]. Subsequent analyses of sequencing data from thousands of individuals confirmed this depletion of common variants from ultraconserved sequences but revealed that the rate of rare polymorphisms is comparable to the genomic average, excluding the possibility that these sites are merely mutational cold spots[4–6]. Together, these observations suggested that ultraconserved sequences are maintained by purifying selection in mammals.

Almost 70% of ultraconserved sequences are noncoding, and many function as distant-acting transcriptional enhancers in embryonic development, as demonstrated through transgenic reporter assays in vivo[7,8]. Deletion of ultraconserved enhancers from the mouse genome yielded viable mice and resulted in surprisingly mild but measurable gene expression changes and developmental phenotypes, consistent with their regulatory function[9–12]. Possible explanations for the relatively subtle nature of the phenotypes include the limited ability of laboratory assays to measure fitness effects relevant in the wild[9,13], as well as the substantial selective constraint that can result, even from minor fitness effects, over many generations[14,15]. These hypotheses can help explain why ultraconserved enhancers are generally conserved, but they do not account for the extreme degree of sequence conservation of these loci. Although multiple functions have been proposed to explain ultraconservation[16,17], the most common function of noncoding ultraconserved sequences directly supported by experimental evidence is embryonic enhancer activity[7,8]. Mutagenesis experiments performed on a small sampling of less well-conserved mammalian enhancers have shown that point mutations tend individually to have little or no effect on enhancer regulatory properties, probably because of the redundancy and/or degeneracy of transcription-factor-binding sites contained within enhancers[18–24]. In contrast, the perfect conservation of ultraconserved enhancers suggests that a mutation in any single one of the base pairs should impact the function of the sequence. These combined findings suggest that the function of ultraconserved enhancers may be 'ultrasensitive' to mutations, that is, even changes of individual base pairs adversely affect their function[16,17]. To test this hypothesis, we performed systematic mutagenesis of almost two dozen ultraconserved enhancers and assessed the resulting effects on enhancer activity in vivo.

Results

Enhancer function of ultraconserved elements is robust to mutagenesis. To explore the impact of mutations on the function of ultraconserved enhancers, we subjected 23 independent ultraconserved

[1]Environmental Genomics & System Biology Division, Lawrence Berkeley National Laboratory, Berkeley, CA, USA. [2]Department of Psychiatry, Neuroscience Program, UCSF Weill Institute for Neurosciences, and the Nina Ireland Laboratory of Developmental Neurobiology, University of California, San Francisco, San Francisco, CA, USA. [3]Comparative Biochemistry Program, University of California, Berkeley, Berkeley, CA, USA. [4]US Department of Energy Joint Genome Institute, Berkeley, CA, USA. [5]School of Natural Sciences, University of California, Merced, Merced, CA, USA. [6]Present address: Department of Developmental & Cell Biology, Department of Ecology & Evolutionary Biology, University of California, Irvine, Irvine, CA, USA. ✉e-mail: avisel@lbl.gov; lapennacchio@lbl.gov; dedickel@lbl.gov

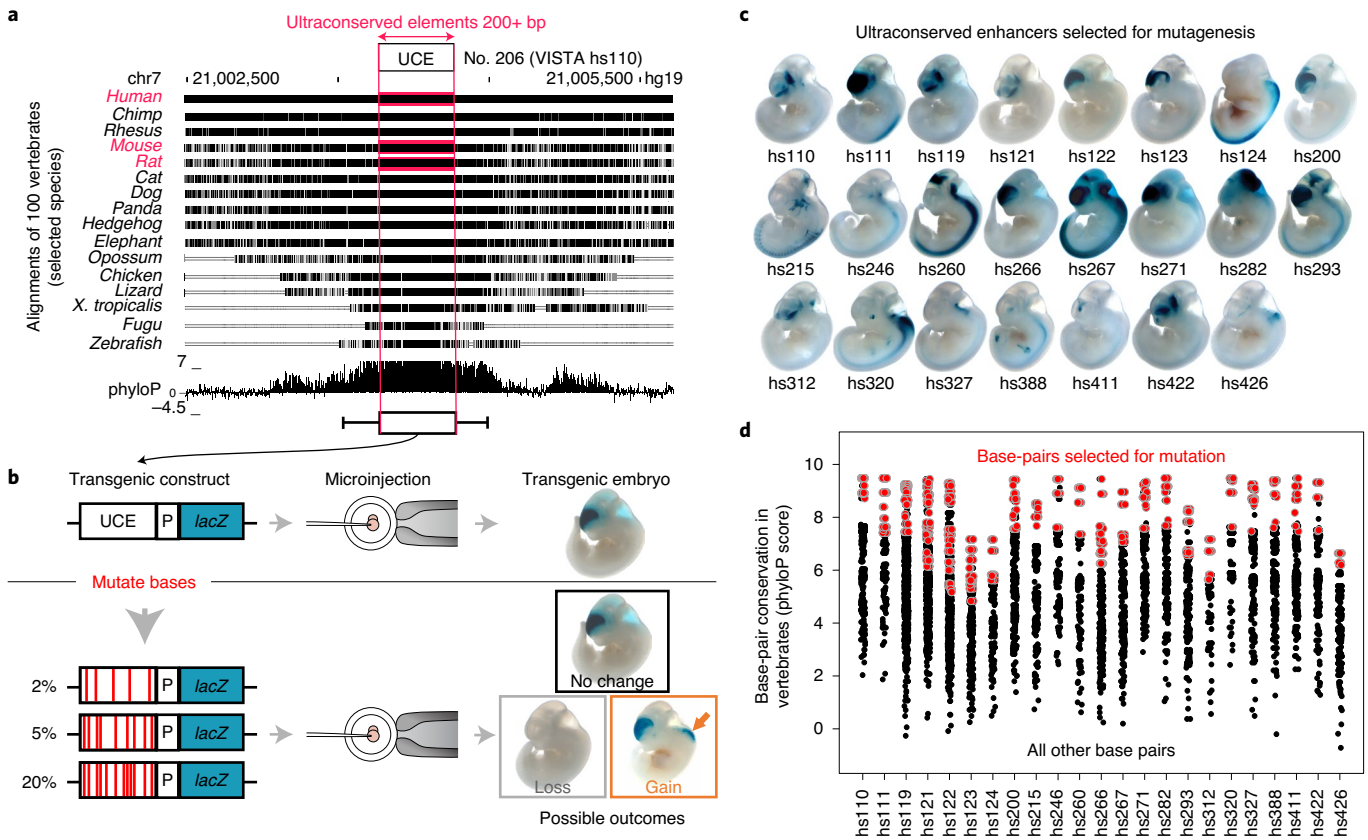

Fig. 1 | Study overview. a, Human–rodent ultraconserved elements showing a high degree of conservation across other sequenced vertebrate genomes. UCE, ultraconserved element. **b**, Study design for mouse transgenic reporter assays to reveal whether mutations in ultraconserved enhancers impact their activity. P, promoter. **c**, Activity of the human reference allele of 23 ultraconserved enhancers selected for mutagenesis. All elements were tested with a CRISPR-assisted, site-specific mouse transgenic reporter assay at mouse e11.5 except hs124, which was tested at e12.5 in the first round of mutagenesis. **d**, Conservation of all human–rodent ultraconserved base pairs within the selected 23 ultraconserved enhancers across 100 sequenced vertebrate genomes (phyloP score obtained from UCSC phyloP100way track). Base pairs selected for mutagenesis are highlighted in red. More details on selecting base pairs for mutagenesis can be found in Extended Data Fig. 1a and Supplementary Fig. 2.

sequences with robust enhancer activity during embryonic development[7,8] to varying levels of mutation (Fig. 1b). The 23 enhancers are active in various tissues, most frequently in subregions of the developing brain, and contain 201–770 bp of ultraconserved sequence, usually embedded within larger blocks of moderately conserved sequence (Fig. 1a,c). For mutagenesis, we prioritized base pairs perfectly conserved across the human, mouse and rat reference genomes that, in addition, had a high level of evolutionary conservation among ~100 sequenced vertebrate genomes, along with nucleotides within predicted conserved transcription-factor-binding sites[25,26]. Otherwise, mutations were evenly distributed across the ultraconserved core of each enhancer, with ~89% of introduced mutations not overlapping a reported human variant (Fig. 1d and Extended Data Fig. 1). In total, we mutagenized 1,547 ultraconserved base pairs within 23 enhancers, generating 74 separate mutant alleles with 2%, 5% or 20% of ultraconserved base pairs mutated. Each allele was tested for in vivo enhancer activity using a CRISPR (clustered regularly interspaced short palindromic repeats)-assisted, site-specific mouse transgenic reporter assay that substantially improves transgenic efficiency and minimizes ectopic reporter expression associated with random transgene integration[24]. Transgenic embryos were scored for reporter gene expression by multiple annotators blinded to the type of allele tested (that is, reference or mutant alleles; see Extended Data Fig. 2 and Methods for details).

We next classified the robustness of ultraconserved enhancers to mutation by comparing the strength and reproducibility of patterns driven by mutant alleles with those produced by the reference enhancer allele (Fig. 2a). Most ultraconserved enhancers (19/23, 83%) were robust to mutagenesis, showing normal tissue specificity, strength and spatial boundaries of enhancer activity for at least one of the mutation alleles tested (Fig. 2b and Extended Data Fig. 3a). For 44% of enhancers (10/23), normal activity was maintained for at least one allele with 5% of ultraconserved base pairs mutated. In one extreme case (hs111), residual enhancer activity in the expected tissue was observed even after mutation of 20% of base pairs (Fig. 2b). For this enhancer, activity was fully abolished after mutation of all base pairs conserved across ~100 sequenced vertebrate genomes[25] (59% of ultraconserved base pairs, Supplementary Fig. 1). Only 4 of 23 (17%) ultraconserved enhancers showed loss of activity with all mutagenesis alleles tested. Although assessing only a subset of all possible variants, our combined results indicate that ultraconserved enhancers commonly maintain their regular activity upon mutagenesis, supporting their perfect conservation not being solely explained by the transcriptional enhancer functions observable in transgenic in vivo assays at the embryonic day 11.5 (e11.5) developmental stage.

To better understand why some of the tested mutation haplotypes decreased or eliminated enhancer activity, whereas many had no effect, we examined sequence characteristics of tested alleles in more detail. There were no substantial differences in the lengths

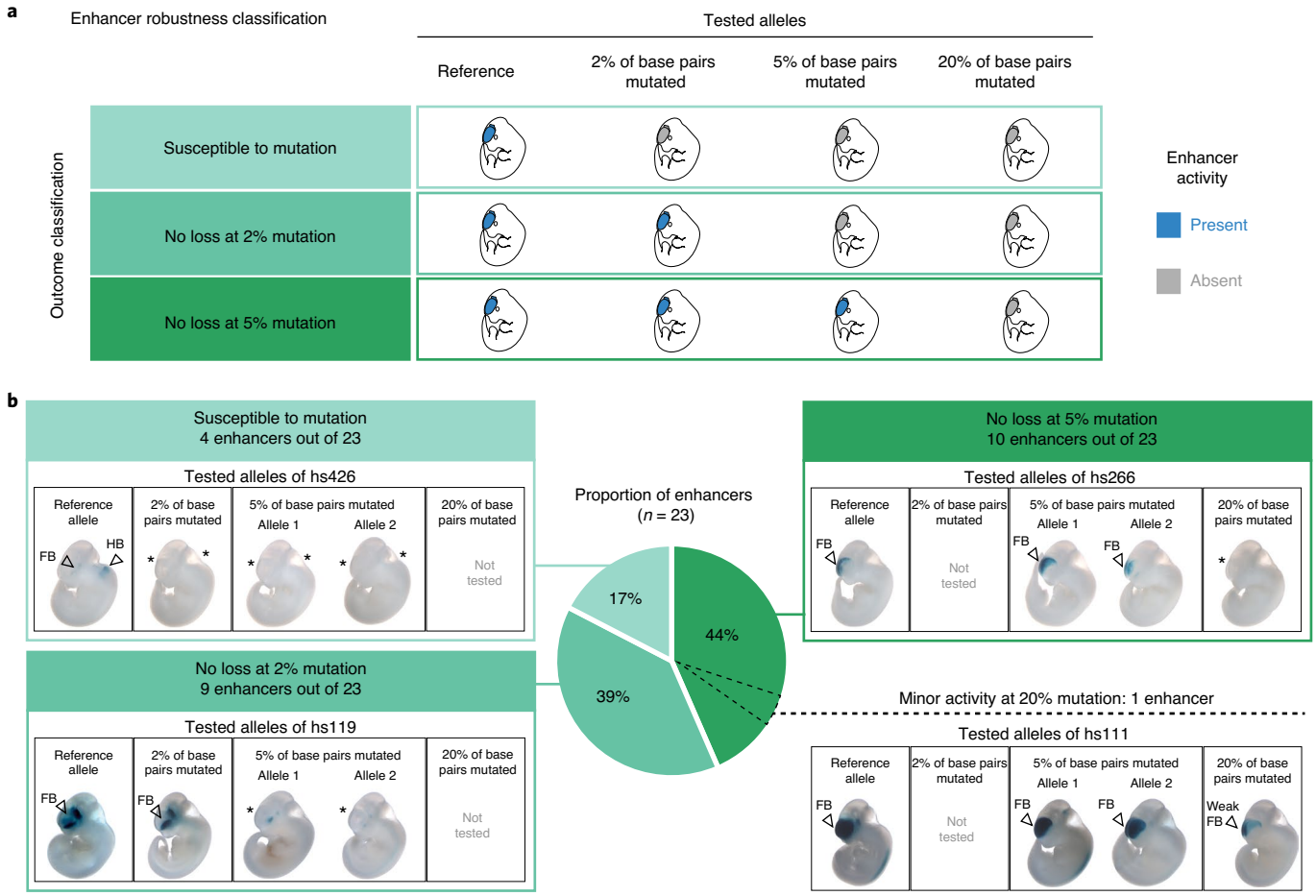

Fig. 2 | Ultraconserved enhancers are mostly robust to mutagenesis. a, Schematic of the possible functional outcomes of enhancer mutagenesis. **b**, Distribution of 23 ultraconserved enhancers across the three bins of enhancer mutagenesis outcomes. Representative embryo images are shown for each tested allele of three example enhancers (boxes in shades of green). In one case (hs111, bottom right), residual enhancer activity was still observed after mutating 20% of ultraconserved base pairs. Data for all 23 enhancers are provided in Extended Data Fig. 3a, with *P* values in Supplementary Table 1. Examples of scoring guidelines are described in Extended Data Fig. 2, with scoring data for all 23 enhancers in Supplementary Fig. 1. The e11.5 embryos have a crown–rump length of 6 mm on average. The asterisk indicates a loss of LacZ staining in the mutant allele. FB, forebrain; HB, hindbrain.

of ultraconserved sequences between enhancers that were either susceptible or robust to mutagenesis (Extended Data Fig. 3b). Consistent with a previous report[27], ultraconserved noncoding sequences, as a class, were enriched for AT-rich motifs of developmental transcription factors from the HOXB, SOX, LHX, DLX and other families (Extended Data Fig. 4a). In agreement, >80% of the ultraconserved enhancers that we selected for mutagenesis are bound by DLX transcription factors in mouse brain at several developmental time points (Extended Data Fig. 5b). We examined whether mutations from loss-of-function alleles could be disproportionately disrupting specific developmental transcription factor motifs. Indeed, motif enrichment analysis of *k*-mers centered on base pairs selected for mutagenesis showed that mutations from loss-of-function alleles were more likely to fall within binding sites for SOX, LHX and DLX family members, among other developmental transcription factors (Extended Data Fig. 4b). In contrast, mutations from alleles with no loss in enhancer activity were enriched in different sequence motifs, including binding sites for the transcriptional repressor MSC (Extended Data Fig. 4b). Comparison of multiple 5% mutated alleles of the same enhancer did not reveal any difference in the total number of affected transcription factor motifs between alleles with and those without observed changes in enhancer activity (Extended Data Fig. 4c). Finally, we examined whether alleles that retained enhancer activity had an enrichment of mutations in potentially redundant transcription factor motifs, that is, motifs that appear more than once in the same enhancer. On average, 48% of transcription factor motifs appeared in each enhancer sequence only once, with the remainder appearing multiple times. The percentage of redundant motifs overlapping introduced mutations was not on average higher for alleles that retained enhancer activity, nor were unique motifs disproportionately mutated in alleles that lost enhancer activity (Extended Data Fig. 4d). Collectively, these results suggest that, although some developmental transcription-factor-binding sites within ultraconserved enhancers are critical for enhancer function, many ultraconserved base pairs can be mutated with no apparent loss of enhancer activity.

Mutation of ultraconserved bases rarely leads to gain of enhancer function. An alternative hypothesis to explain the ultraconservation of enhancers is that these sites may be highly susceptible to gains of function, where mutations may result in enhancer activity in additional tissues or cell types[11]. Considering that many ultraconserved enhancers are enriched near developmentally expressed transcription factors[1], which are often regulated by multiple, seemingly redundant, enhancers[28], such misexpression may be more deleterious than loss-of-function mutations. To explore this possibility,

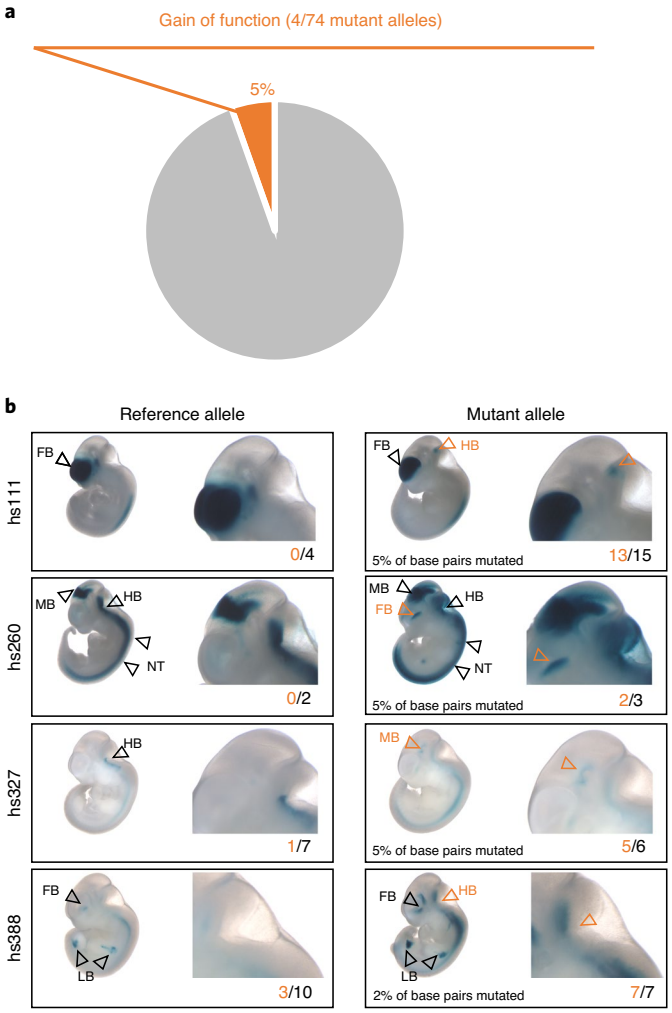

Fig. 3 | Gain of function is uncommon among mutated alleles of ultraconserved enhancers. a, Proportion of gain-of-function alleles detected among all different mutant alleles of 23 ultraconserved enhancers. **b**, Images of representative transgenic embryos from four gain-of-function alleles resulting from ultraconserved enhancer mutagenesis. Numbers of embryos surveyed are displayed under the images, with those in orange representing embryos with gain-of-reporter expression. *P* values are provided in Supplementary Table 2. The e11.5 embryos have a crown–rump length of 6 mm on average. LB, limb; MB, midbrain; NT, neural tube.

we examined the 74 different mutant alleles for the 23 ultraconserved enhancers tested in the present study for any enhancer activity that was not observed for the reference allele. Only 4 of the 74 mutant alleles showed gain of transgene activity in vivo (Fig. 3a). These gain-of-function activities fell into two categories: mutations in two ultraconserved enhancers (hs111 and hs260) led to ectopic activity in new tissues, whereas mutations in two other ultraconserved enhancers (hs327 and hs388) resulted in a more reproducible reporter staining in tissues with existing enhancer activity (Fig. 3b). These results indicate that gains of enhancer function due to mutations in ultraconserved sequences are generally possible and may contribute to the selective constraint on individual base pairs, but overall are uncommon and, therefore, appear unlikely to be the main driver of ultraconservation.

Differential impact on enhancer activity across multiple developmental stages. Many of the ultraconserved enhancers investigated in the present study show tissue-specific enrichment in the enhancer activity-associated histone mark, H3K27ac, across multiple stages of mouse development, suggesting extended activity windows beyond e11.5 (Extended Data Fig. 5a). To assess whether mutations not affecting the enhancer activity at e11.5 may instead alter activity at other developmental stages, we examined a subset of the reference and mutant alleles in transgenic reporter assays at a later embryonic stage. At e14.5, we re-tested the reference alleles for the ten enhancers in the no loss of activity at 5% category (dark green in Fig. 2b and Extended Data Fig. 3a). All ten reference alleles were, indeed, active enhancers at e14.5 (Fig. 4). We then compared this activity with e14.5 results for the 5% mutated alleles that had retained enhancer activity at e11.5, with the exception of hs111, where the 20% mutated allele was tested (Fig. 4a). Five of the nine 5% mutant alleles tested showed no loss of enhancer activity at e14.5 (Fig. 4b). Two alleles (hs266 and hs271) showed minor reductions in activity at e14.5 (Fig. 4b), and two (hs200 and hs246) showed complete loss of activity in one structure (neural tube and forebrain, respectively), while retaining activity in other structures (forebrain and hindbrain/neural tube, respectively), indicating a pronounced stage- and tissue-specific difference in the impact of these mutations (Fig. 4b). Gain-of-function activities were restricted to a mutated allele of hs260, which caused gain of enhancer activity in the forebrain at e14.5, just like at e11.5, and in addition showed more reproducible activities in the midbrain, hindbrain and neural tube at e14.5 (Figs. 3b and 4b). The 20% mutated allele of hs111 recapitulated the reduced but not abolished activity observed at e11.5 (Figs. 2b and 4c). In summary, these results suggest that some mutations have differential effects on enhancer activity at different time points, revealing an additional source of possible sequence constraint. However, considering such changes were absent in more than half (5/9) of the cases examined, despite the relatively high mutation rate of 5%, this effect appears unlikely to be the sole source of the extreme sequence constraint observed at ultraconserved enhancers. Importantly, these findings underscore the need to examine multiple developmental stages or contexts when considering the effects of mutations on the activity of enhancers.

Robustness of ultraconserved enhancer function in native genomic context. Our results from transgenic reporter assays indicate that ultraconserved enhancers are overall remarkably robust to mutations, but also identify multiple cases in which mutations caused a reduction or loss of enhancer activity. However, the transgenic assays were limited to one to two specific stages of embryonic development and tested each enhancer's activity outside of its endogenous context. To assess whether activity changes observed in transgenic reporter assays correctly predict whether ultraconserved enhancers are functionally robust or sensitive to mutations within their native genomic environment, we generated stable knock-in mouse lines for three different mutagenesis alleles of two ultraconserved enhancers (Figs. 5a and 6a, and Extended Data Fig. 6). Both enhancers are located near and regulate the aristaless-related homeobox (*Arx*) gene on chromosome X, and individual deletions of either of these enhancers were previously shown to cause phenotypic changes in the brain[9]. First, we replaced the mouse orthologue of enhancer hs122 with a 5% mutagenized allele that inactivated enhancer function in the transgenic reporter assay (Fig. 5b and Extended Data Fig. 7a). *Arx* RNA in situ hybridization (ISH) on forebrain tissue sections from hemizygous knock-in male embryos revealed a reduction in *Arx* expression in the caudal dorsal forebrain compared with wild-type littermate controls (Extended Data Fig. 8a), which is similar to reductions observed for hs122-null embryos[9]. Also, as expected, brain sections from postnatal hemizygous knock-in males showed the same abnormalities to the hippocampus (in the dentate gyrus and CA3) observed on complete deletion of the enhancer, including a 20% length reduction and disorganized structure of the dentate gyrus relative to wild-type

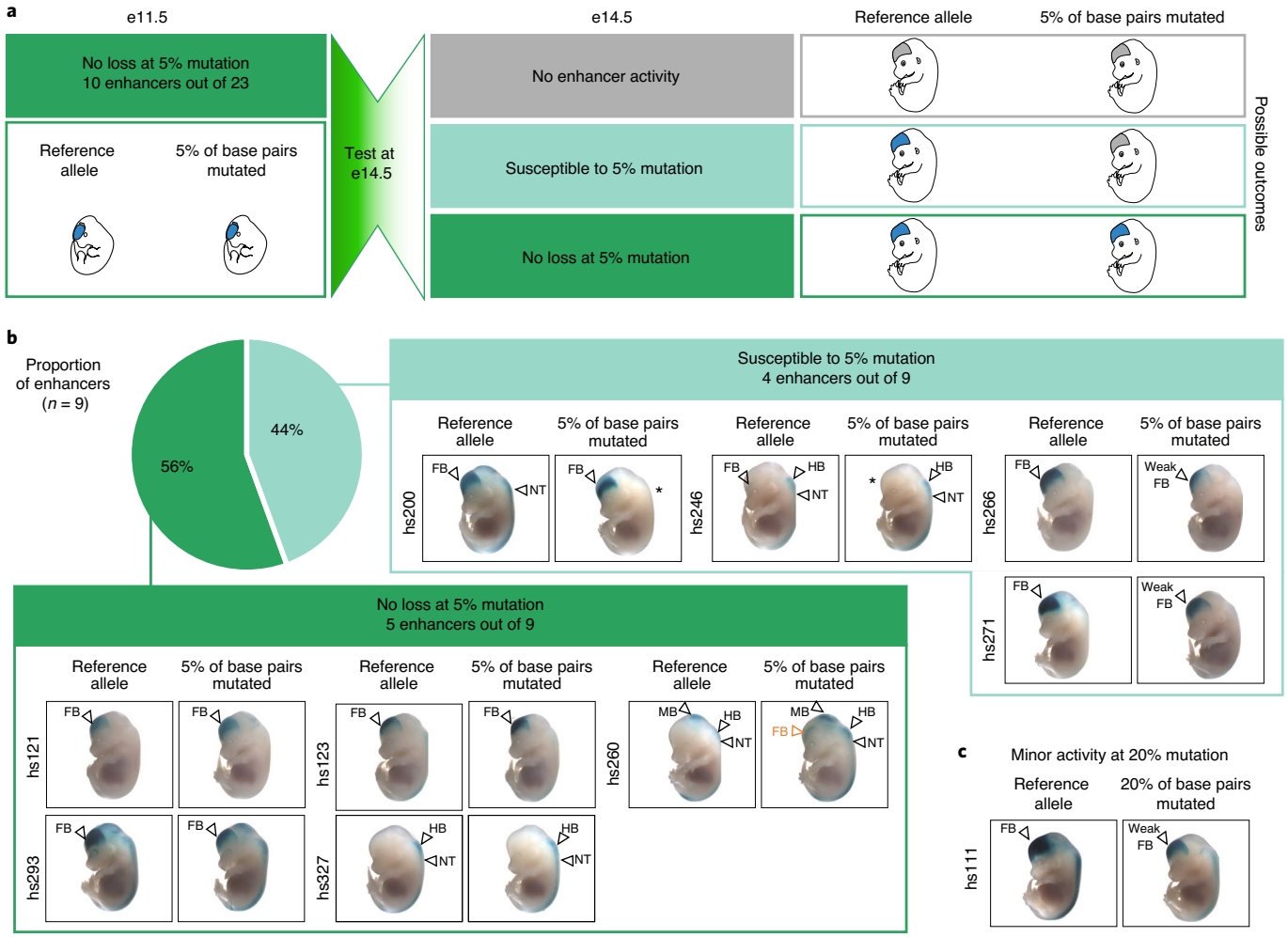

Fig. 4 | Mutagenesis of ultraconserved enhancers at a later stage of development recapitulates earlier results for most tested enhancers but exposes susceptibility to mutations for some. a, Schematic of experimental design to test ultraconserved enhancers shown to be robust to 5% mutagenesis at e11.5, at a later developmental stage of e14.5, and the possible functional outcomes. **b**, Transgenic assay results for nine ultraconserved enhancers at e14.5. See Supplementary Fig. 1 for reproducibility of LacZ staining among individual transgenic embryos from each enhancer allele. The * indicates a loss of LacZ staining in the mutant allele. **c**, Transgenic assay results for hs111 at e14.5.

littermate controls ($P=0.02109$ by two-tailed, paired Student's *t*-test; Fig. 5b and Extended Data Fig. 9).

Next, we replaced ultraconserved enhancer hs121 with two different 5% mutagenized alleles: hs121^{mut1}, which showed normal enhancer activity in transgenic assays; or hs121^{mut2}, which was inactive (Fig. 6b and Extended Data Fig. 7b). To determine the phenotypic impact of these alleles, we assessed the density of vasointestinal peptide-positive (VIP$^+$) interneurons in the cortex of postnatal mice, because deletion of hs121 is known to cause an increased density of these neurons[9]. Replacing the endogenous mouse hs121 enhancer with hs121^{mut1} did not result in any changes to VIP$^+$ neuron density ($P=0.8621$ by a two-tailed, paired Student's *t*-test; Fig. 6b and Extended Data Fig. 10). In contrast, replacement with hs121^{mut2} caused increased density of VIP$^+$ interneurons compared with wild-type littermates (21% increase, $P=0.02624$ by a two-tailed, paired Student's *t*-test; Fig. 6b and Extended Data Fig. 10).

These observations highlight the concordance of enhancer activity in transgenic reporter assays with the phenotypic consequences of mutating ultraconserved enhancers at their endogenous loci. Results for the two inactive alleles confirm that mutations in ultraconserved enhancers can cause deleterious phenotypes. However, the absence of brain phenotypes with one mutant allele (mut1) of hs121 provides further support for the notion that the regulatory activities of some ultraconserved enhancers are surprisingly robust to sequence changes. The absence of a brain phenotype in adult mice with this mutated allele introduced into the endogenous hs121 sequence suggests that this allele remained functional throughout developmental time points that we did not test in our transgenic assays, underscoring the developmental timing of enhancer activity not being the sole explanation of ultraconservation.

Discussion

We performed a detailed assessment of how mutations in ultraconserved enhancers affect their respective regulatory activities, taking advantage of a targeted transgene knock-in approach[24] with high sensitivity for detecting activity changes in vivo. Although the perfect sequence conservation of ultraconserved enhancers may suggest that most or all of their base pairs are required for normal enhancer function, we observed that most ultraconserved enhancers that we tested (83%) at e11.5 were functionally robust to some level of mutagenesis, and almost half showed no loss of activity even after

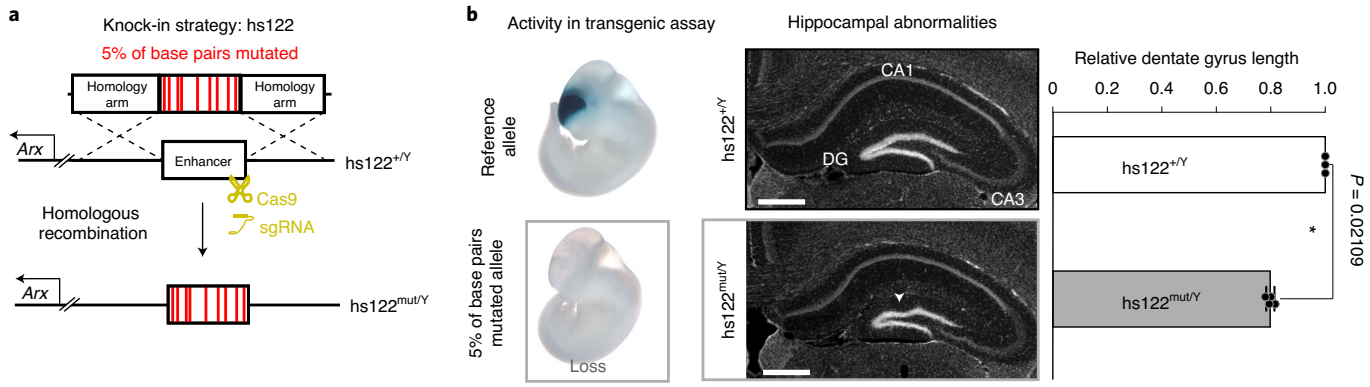

Fig. 5 | Mutagenesis of endogenous ultraconserved enhancer hs122 causes brain phenotypes. a, Schematic of the knock-in strategy used to replace the endogenous mouse allele of ultraconserved enhancer hs122 with an allele in which 5% of base pairs were mutated. **b**, Left: transgenic assay results for hs122 reference and mutated enhancer alleles. Center: rostral coronal cross-sections of postnatal hippocampus from a wild-type male control ($hs122^{+/Y}$) and a hemizygous mutant knock-in littermate ($hs122^{mut/Y}$) are shown. Replacement of the endogenous mouse hs122 allele with a mutagenesis allele that inactivated enhancer activity in the transgenic assay results in a smaller dentate gyrus (DG) with disorganized appearance (white arrowhead). CA1/3, Cornu Ammonis areas 1 and 3. Scale bars, 500 µm. Right: dentate gyrus length for knock-in allele normalized to wild-type littermate controls. Bars indicate group means, with individual points showing biological replicates ($n = 3$ for wild-type, $n = 4$ for knock-in). Error bars are mean ± s.d. and a two-tailed, paired Student's *t*-test was used. $^*P < 0.05$. Images for all replicates are in Extended Data Fig. 9 and raw measurements in Supplementary Table 3.

mutation of 5% of ultraconserved base pairs. Likewise, mutations rarely resulted in new enhancer activities in other tissues, suggesting that deleterious gain-of-function effects do not explain the conservation of most ultraconserved base pairs. Additional transgenic assays for nine ultraconserved enhancers and their mutated alleles at a later developmental stage (e14.5) confirmed robustness to mutagenesis for the majority (56%) of tested elements. These results relied on a CRISPR-assisted, site-specific mouse transgenic reporter assay that minimizes ectopic reporter expression and results in far lower variability between independent replicate embryos with the same enhancer–reporter construct[24]. For example, across all 121 transgenic experiments (distinct allele and developmental stage combinations) reported herein, 64 resulted in all replicate embryos having identical enhancer activity patterns (Supplementary Fig. 1). In addition, all 5 expert annotators who carried out blinded and independent scoring of embryos unanimously agreed on annotations for 75% of all 690 embryos scored for the present study. This increased consistency allows for the identification of altered enhancer activity with smaller sample sizes than traditional random transgenesis assays (for example, compare results with those of refs. [29] and [30]). As the data herein show, the site-directed transgenic assay is a powerful technique to identify both quantitative and spatial changes in in vivo enhancer activity at the scale of a whole organism. However, we cannot exclude the possibility that introduced mutations had subtle effects on enhancer activity below the threshold of detection of the assay.

As a result of the inherent limitations of transgenic assays, we also used a knock-in approach to investigate whether mutations had similar effects on ultraconserved enhancer activities in their endogenous positions, and to examine their phenotypic consequences beyond gene expression. Mutations that eliminate the activity of the ultraconserved brain enhancers in the transgenic reporter assay indeed caused phenotypes recapitulating those produced by deleting the respective enhancers. At the same time, mutations that did not affect an ultraconserved enhancer's activity in the transgenic assay also failed to elicit an abnormal brain phenotype in stable knock-in animals, thus confirming the robustness of that ultraconserved enhancer to mutagenesis in its native genomic context. Together, these results show that, although sequence changes in ultraconserved enhancers can affect their regulatory activities and cause organismal phenotypes, most tested ultraconserved enhancers can still activate gene expression on mutagenesis.

It has been suggested that the unusually high degree of evolutionary constraint on ultraconserved elements may result from the involvement of nearly all of their base pairs in DNA–protein interactions[17] or multiple overlapping constraints (for example, transcription-factor-binding sites overlapping with RNA structural constraints)[16]. Supporting this, cell culture experiments indicate that transcription factors and chromatin remodelers densely occupy ultraconserved elements[31]. The overall robustness of ultraconserved enhancers to mutagenesis in the present study shows that, although such interactions may occur, not all are required for normal enhancer function. Therefore, this model alone does not provide a direct explanation for the extreme conservation of noncoding ultraconserved sequences. Although it is plausible to assume that molecular functions, in addition to the known developmental enhancer activities, may be associated with noncoding ultraconserved sequences, their exact nature remains elusive because experimental evidence demonstrating such functions (for example, in three-dimensional genome organization) is limited to a few anecdotal examples[17,32]. Although such a role of ultraconserved sequences is, in principle, conceivable, the absence of binding by the chromatin architectural protein CTCF in most of the ultraconserved noncoding sequences tested in the present study suggests that a role in genome organization is not a probable explanation for their extreme conservation (Extended Data Fig. 5c). As our study primarily relied on techniques to assess the role of ultraconserved sequences in gene expression activation, we cannot exclude effects of mutagenesis on nonenhancer functions. We also cannot exclude that mutations may affect the activities of the tested enhancers at other developmental time points, or in tissues and cell types not investigated in our reporter and knock-in assays (Extended Data Fig. 5a). Although this is possible, the apparent absence of a phenotype from the knock-in of one mutated allele of hs121, which also did not alter reporter gene expression in transgenic assays at e11.5 and e14.5, suggests that this enhancer's activity was unaffected at other, unexamined, developmental time points. In summary, our results indicate that the known embryonic enhancer activities of ultraconserved sequences do not show an abnormally high sensitivity to sequence changes. This suggests that either mutations

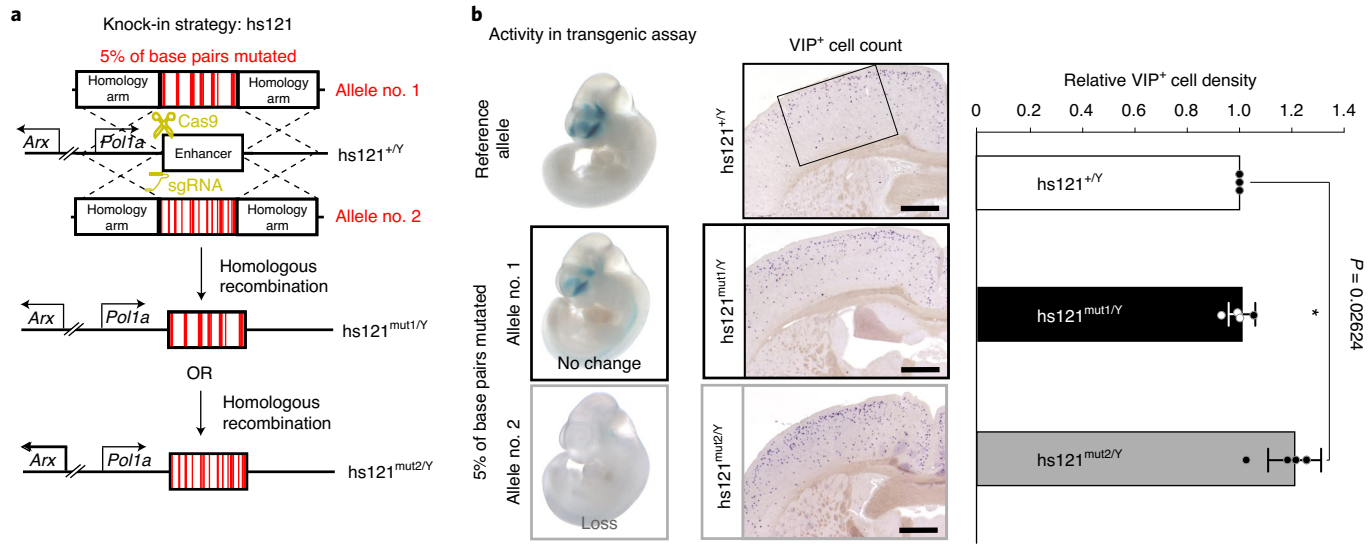

Fig. 6 | Mutagenesis of endogenous ultraconserved enhancer hs121 corroborates transgenic assay results. a, Schematic of the knock-in strategy used to replace the endogenous mouse allele of ultraconserved enhancer hs121 with alleles in which 5% of all base pairs were mutated. **b**, Left: transgenic assay results for hs121 reference and mutated enhancer alleles. Center: coronal sections through the cortex of postnatal wild-type control ($hs121^{+/Y}$) and hemizygous mutant knock-in males ($hs121^{mut1/Y}$ and $hs121^{mut2/Y}$) labeled for VIP are shown. Mutagenesis of hs121 results in a higher density of VIP^+ cells in the brain only for mutations that abolished enhancer activity in the transgenic assay. The rectangle shown in the image of the $hs121^{+/Y}$ brain marks the area used to count the cells. Scale bars, 1 mm. Right: density of VIP^+ neurons (cells mm^{-2}) for the two knock-in alleles normalized to wild-type littermate controls. Bars indicate group means, with individual points showing biological replicates ($n = 3$ for wild-type, $n = 4$ for knock-in). Error bars are mean ± s.d. and a two-tailed, paired Student's *t*-test was used. $^*P < 0.05$. Images for all replicates are in Extended Data Fig. 10 and raw measurements in Supplementary Table 4.

in ultraconserved enhancers result in very subtle but still selectively disadvantageous effects on gene expression, or additional, yet-to-be-identified, regulatory or nonregulatory functions of these sequences contribute to their extreme conservation in evolution.

Online content

Any methods, additional references, Nature Research reporting summaries, extended data, supplementary information, acknowledgements, peer review information; details of author contributions and competing interests; and statements of data and code availability are available at https://doi.org/10.1038/s41588-021-00812-3.

Received: 14 May 2020; Accepted: 4 February 2021;
Published online: 29 March 2021

References

1. Bejerano, G. et al. Ultraconserved elements in the human genome. *Science* **304**, 1321–1325 (2004).
2. Hecker, N. & Hiller, M. A genome alignment of 120 mammals highlights ultraconserved element variability and placenta-associated enhancers. *Gigascience* **9**, giz159 (2020).
3. Katzman, S. et al. Human genome ultraconserved elements are ultraselected. *Science* **317**, 915 (2007).
4. Drake, J. A. et al. Conserved noncoding sequences are selectively constrained and not mutation cold spots. *Nat. Genet.* **38**, 223–227 (2006).
5. Ovcharenko, I. Widespread ultraconservation divergence in primates. *Mol. Biol. Evol.* **25**, 1668–1676 (2008).
6. Habic, A. et al. Genetic variations of ultraconserved elements in the human genome. *OMICS* **23**, 549–559 (2019).
7. Pennacchio, L. A. et al. In vivo enhancer analysis of human conserved non-coding sequences. *Nature* **444**, 499–502 (2006).
8. Visel, A. et al. Ultraconservation identifies a small subset of extremely constrained developmental enhancers. *Nat. Genet.* **40**, 158–160 (2008).
9. Dickel, D. E. et al. Ultraconserved enhancers are required for normal development. *Cell* **172**, 491–499 e15 (2018).
10. Nolte, M. J. et al. Functional analysis of limb transcriptional enhancers in the mouse. *Evol. Dev.* **16**, 207–223 (2014).
11. Ahituv, N. et al. Deletion of ultraconserved elements yields viable mice. *PLoS Biol.* **5**, e234 (2007).
12. Gaynor, K. U. et al. Studies of mice deleted for Sox3 and uc482: relevance to X-linked hypoparathyroidism. *Endocr. Connect.* **9**, 173–186 (2020).
13. Chen, C. T., Wang, J. C. & Cohen, B. A. The strength of selection on ultraconserved elements in the human genome. *Am. J. Hum. Genet.* **80**, 692–704 (2007).
14. Kryukov, G. V., Schmidt, S. & Sunyaev, S. Small fitness effect of mutations in highly conserved non-coding regions. *Hum. Mol. Genet.* **14**, 2221–2229 (2005).
15. Keightley, P. D., Kryukov, G. V., Sunyaev, S., Halligan, D. L. & Gaffney, D. J. Evolutionary constraints in conserved nongenic sequences of mammals. *Genome Res.* **15**, 1373–1378 (2005).
16. Siepel, A. et al. Evolutionarily conserved elements in vertebrate, insect, worm, and yeast genomes. *Genome Res.* **15**, 1034–1050 (2005).
17. Harmston, N., Baresic, A. & Lenhard, B. The mystery of extreme non-coding conservation. *Philos. Trans. R. Soc. Lond. B Biol. Sci.* **368**, 20130021 (2013).
18. Patwardhan, R. P. et al. Massively parallel functional dissection of mammalian enhancers in vivo. *Nat. Biotechnol.* **30**, 265–270 (2012).
19. Melnikov, A. et al. Systematic dissection and optimization of inducible enhancers in human cells using a massively parallel reporter assay. *Nat. Biotechnol.* **30**, 271–277 (2012).
20. Dickel, D. E., Visel, A. & Pennacchio, L. A. Functional anatomy of distant-acting mammalian enhancers. *Philos. Trans. R. Soc. Lond. B Biol. Sci.* **368**, 20120359 (2013).
21. Kircher, M. et al. Saturation mutagenesis of twenty disease-associated regulatory elements at single base-pair resolution. *Nat. Commun.* **10**, 3583 (2019).
22. Lettice, L. A., Devenney, P., De Angelis, C. & Hill, R. E. The conserved sonic hedgehog limb enhancer consists of discrete functional elements that regulate precise spatial expression. *Cell Rep.* **20**, 1396–1408 (2017).
23. Canver, M. C. et al. BCL11A enhancer dissection by Cas9-mediated in situ saturating mutagenesis. *Nature* **527**, 192–197 (2015).
24. Kvon, E. Z. et al. Comprehensive in vivo interrogation reveals phenotypic impact of human enhancer variants. *Cell* **180**, 1262–1271 (2020).
25. Karolchik, D. et al. The UCSC table browser data retrieval tool. *Nucleic Acids Res.* **32**, D493–D496 (2004).
26. Hinrichs, A. S. et al. The UCSC genome browser database: update 2006. *Nucleic Acids Res.* **34**, D590–D598 (2006).
27. Chiang, C. W. et al. Ultraconserved elements: analyses of dosage sensitivity, motifs and boundaries. *Genetics* **180**, 2277–2293 (2008).

28. Osterwalder, M. et al. Enhancer redundancy provides phenotypic robustness in mammalian development. *Nature* **554**, 239–243 (2018).
29. Turner, T. N. et al. Genomic patterns of de novo mutation in simplex autism. *Cell* **171**, 710–722.e12 (2017).
30. Fakhouri, W. D. et al. An etiologic regulatory mutation in IRF6 with loss- and gain-of-function effects. *Hum. Mol. Genet.* **23**, 2711–2720 (2014).
31. Viturawong, T., Meissner, F., Butter, F. & Mann, M. A DNA-centric protein interaction map of ultraconserved elements reveals contribution of transcription factor binding hubs to conservation. *Cell Rep.* **5**, 531–545 (2013).
32. McCole, R. B., Erceg, J., Saylor, W. & Wu, C. T. Ultraconserved elements occupy specific arenas of three-dimensional mammalian genome organization. *Cell Rep.* **24**, 479–488 (2018).

Methods

Selection of ultraconserved enhancers for mutagenesis. A list of human–rodent ultraconserved sequences that show in vivo enhancer activity during development was compiled from previous publications[7,8]. From this list, we selected 23 ultraconserved enhancers that showed highly reproducible activity in mouse transgenic enhancer–reporter assays at the e11.5 or e12.5 developmental time point. Enhancer names (hs numbers) used are the unique identifiers from the VISTA Enhancer Browser (https://enhancer.lbl.gov/). The coordinates of ultraconserved enhancers from Visel et al.[8] were converted from hg17 to the hg19 (human) genome assembly using liftOver[26].

Design of mutations to introduce into ultraconserved enhancers. We mutated ultraconserved enhancers at various levels, changing 2%, 5% or 20% of their base pairs. To select which base pairs to mutate, we first looked beyond human and rodent genome conservation to prioritize the nucleotides with the highest conservation across 100 vertebrates using phyloP scores[33] (phyloP100way) from the USCS genome browser[25] (http://hgdownload.cse.ucsc.edu/goldenpath/hg19/phyloP100way). Then we prioritized nucleotides that fall within predicted conserved transcription factor motifs (HMR Conserved Transcription Factor Binding Sites Track on the UCSC genome browser)[26]. Finally, we tried to evenly distribute mutations across the ultraconserved portion of the enhancers. In principle, this prioritization strategy should introduce mutations that have the highest chance of affecting the enhancer function. Extended Data Fig. 1 shows the locations of mutated base pairs for selected ultraconserved enhancers, with data for all 23 enhancers in Supplementary Fig. 2. Supplementary Table 1 contains the coordinates of 23 ultraconserved enhancers used in the present study and FASTA-formatted sequences for the ultraconserved portions of all generated reference and mutant alleles.

Generation of transgenic embryos. All animal work done in the present study was reviewed and approved by the Lawrence Berkeley National Laboratory Animal Welfare and Research Committee. Mice were housed in the animal facility, where their conditions were electronically monitored 24 h per day with daily visual checks by technicians. The facility was also equipped with automatic alarms. Mice were housed in BioBubble Clean Rooms, soft-walled enclosures powered by 80–100 air changes per h of high efficiency particulate air (HEPA) filtration under a light:dark cycle of 12 h:12 h starting at 06:00, at 22–24.4 °C and 30–70% humidity.

Human reference and mutant alleles for all 23 ultraconserved enhancers were tested with site-directed transgenic mouse assays using a minimal promoter of *Shh* and a *lacZ* reporter gene[24]. Reference alleles had previously been tested for enhancer activity using random transgenic methods, and these results are reported elsewhere[7,8]. However, to allow for direct allelic comparisons, we newly performed site-directed transgenic experiments for all reference and mutant alleles as part of the present study. Reference alleles were PCR amplified (primers in Supplementary Table 5) from human genomic DNA. Mutant alleles were assembled from PCR fragments flanking ultraconserved regions and gBlock DNA Fragments (IDT) containing the designed mutations in the ultraconserved sequences. Reference and mutant alleles were cloned into a LacZ reporter vector via Gibson cloning[34] (New England Biolabs). In the final transgenic vectors, the enhancer–promoter–reporter sequence is flanked by homology arms for the site-specific integration of the transgene into the *H11* locus in the mouse genome[24]. Site-specific integration dramatically improves transgenic efficiency and almost eliminates ectopic LacZ staining associated with random transgene integration, allowing for better comparisons between enhancer alleles. Sequences of all constructs were confirmed with Sanger sequencing. Transgenic mice were generated using the *Mus musculus* FVB strain via a CRISPR–Cas9 microinjection protocol, as described previously[24]. Briefly, Cas9 protein (Integrated DNA Technologies, catalog no. 1081058) at a final concentration of 20 ng μl^{-1} was mixed with single guide (sg)RNA targeting the *H11* locus (50 ng μl^{-1}) and transgenic vector (25 ng μl^{-1}) in microinjection buffer (10 mM Tris, pH 7.5 and 0.1 mM ethylenediaminetetraacetic acid). The mix was injected into the pronuclei of fertilized FVB embryos, obtained from the oviducts of superovulated 7- to 8-week-old FVB females mated to FVB stud males. The injected embryos were then cultured in M16 medium supplemented with amino acids at 37 °C under 5% CO_2 for ~2 h. The embryos were subsequently transferred into the uteri of pseudo-pregnant CD-1 surrogate mothers. F_0 embryos were collected for staining at e11.5 (e12.5 for the hs124 enhancer), with ten enhancers additionally tested at e14.5. LacZ staining was performed as previously described[35]. Briefly, embryos were washed in cold 1× phosphate-buffered saline (PBS) three times for ~5 min each, followed by fixation with 4% paraformaldehyde (PFA) while tumbling for 30 min at room temperature. The embryos were washed in embryo wash buffer (2 mM magnesium chloride (Ambion, catalog no. AM9530), 0.02% NP-40 substitute (Fluka, catalog no. 74385), 0.01% deoxycholate (Sigma-Aldrich, catalog no. D6750) diluted in 0.1 M phosphate buffer, pH 7.3) three times for 30 min each at room temperature and transferred into freshly made X-gal staining solution (4 mM potassium ferricyanide (Sigma-Aldrich, catalog no. P3667), 4 mM potassium ferrocyanide (Sigma-Aldrich, catalog no. P9387), 20 mM Tris, pH 7.5 (Invitrogen, catalog no. 15567027), 1 mg ml^{-1} of X-gal (Sigma-Aldrich, catalog no. B4252)) to incubate overnight while tumbling at room temperature. The next day, embryos were washed with 1× PBS three times for at least 30 min each and stored in 4% PFA at 4 °C. The embryo sample sizes were determined empirically based on our experience performing >4,000 transgenic enhancer assays (VISTA Enhancer Browser: https://enhancer.lbl.gov). The embryos were genotyped as previously described[24], and those negative for transgene integration into the *H11* locus were excluded from further analysis, along with embryos that were not at the correct developmental stage. On average, we obtained 5 correctly targeted transgenic embryos per tested allele (range 2–16). The exact number of embryos for each allele is reported in Supplementary Table 1, and images of all embryos included in the study are shown in Supplementary Fig. 1.

Scoring the strength of ultraconserved enhancer activity in transgenic embryos. We used the spatial pattern and intensity of LacZ staining in an embryo as a proxy for enhancer activity. A schematic of the scoring protocol is shown in Extended Data Fig. 2, and the scoring results for all embryos and enhancers are included in Supplementary Fig. 1. The embryos were imaged with a Leica MZ16 microscope and a Leica DFC420 digital camera using consistent lighting conditions. Reference and mutant alleles of the same enhancer were imaged on the same day. First, for each of the 23 tested ultraconserved enhancers, we selected representative embryo images as examples of enhancer activity levels: strong, weak or absent. For cases of gain of enhancer function, we classified enhancer activity as present or absent. To score the enhancer activity, we then randomly aggregated embryo images from the reference and all tested mutant alleles for one enhancer together (16–45 embryo images per enhancer locus). Five reviewers, who were blinded to the genotype of the enhancer alleles, were first shown the example images of the different enhancer activity levels. The reviewers were then shown all the randomized embryo images for that enhancer one by one for scoring. The reviewers independently recorded their score for each embryo image as strong, weak or absent, and present or absent in gain-of-function cases. The strength of enhancer activity in each transgenic embryo was annotated based on majority rule among the five reviewers.

Generation of enhancer knock-in mice. We introduced mutations into the endogenous mouse orthologues of the hs122 and hs121 enhancers, changing 5% of ultraconserved base pairs at a time. The mutant enhancer alleles were knocked in via homologous recombination to replace the reference allele. SgRNAs targeting the endogenous hs122 enhancer (5′-TAACCACTAAGCTAATAAGT[AGG]-3′, with AGG as the protospacer adjacent motif (PAM) sequence) and the hs121 enhancer (5′-AGGGGACTCGGGTTAAATGC[TGG]-3′, with TGG as the PAM sequence) were designed with CHOPCHOP[36] and ordered from IDT as Alt-R CRISPR–Cas9 (cr)RNAs. To generate homologous recombination templates, we synthesized gBlock DNA Fragments (IDT) containing the mutated ultraconserved sequences of either hs122 (one mutant allele with 5% of base pairs mutated) or hs121 (two mutant alleles with 5% of base pairs mutated each). Flanking mouse sequences (~2 kb) were amplified from mouse genomic DNA to create homology arms for site-specific integration; cloning primers are listed in Supplementary Table 6. For each enhancer mutant allele, gBlock DNA Fragments and amplified homology arms were cloned together into the pCR4-TOPO backbone (Thermo Fisher Scientific) via Gibson (New England Biolabs) cloning[34]. The hs122 sgRNA overlaps 7-bp changes in the hs122 mutant allele, avoiding the need to further mutagenize the sgRNA target site in the homologous recombination repair template. The hs121 sgRNA is located 115 bp away from the ultraconserved sequence; we mutated its PAM sequence (TGG>TAG) in the two repair templates carrying the mutated alleles of the hs121 enhancer to avoid their cleavage by CRISPR–Cas9. Knock-in mice were generated via the CRISPR–Cas9 microinjection protocol described above. Founder (F_0) pups were checked for correctly targeted knock-in alleles with PCR amplification of overlapping fragments spanning the entire homologous recombination region, starting from the flanking genomic DNA on the 5′ and 3′ sides, as schematically represented in Extended Data Fig. 4. This was followed by Sanger sequencing. Genotyping primers are provided in Supplementary Table 6. F_0s were also tested for the absence of the vector backbone. Multiple founders with a precise recombination of the mutated enhancer sequence into the endogenous hs122 and hs121 loci were obtained (Supplementary Table 7). The knock-in lines were expanded and maintained by outcrossing mutation carriers with wild-type FVB animals to minimize the likelihood of a line harboring an off-target mutation.

Sample selection for phenotyping of the mutated enhancer knock-in lines. The hs122 and hs121 enhancers and their target gene, *Arx*, reside on the X chromosome, so phenotyping was performed exclusively on male mice. Male mice missing the hs122 enhancer entirely display defects to the hippocampus, whereas male mice hemizygous for the hs121 enhancer deletion show abnormalities in neuronal cell populations[9]. Therefore, we performed the same neurological phenotyping as was done in that previous study. All mice used for phenotyping were either F_1 or F_2 generation, derived from crossing either female F_0 knock-in founders or heterozygous F_1 females to wild-type FVB males. Knock-in males were phenotyped using wild-type male littermates as controls. Details on all phenotyped animals are provided in Supplementary Tables 3 and 4.

Brain sectioning. Mice were anesthetized with an intraperitoneal pentobarbital injection (1 μl of a 50 μg μl^{-1} solution diluted in saline per 1 g of an animal's weight) and perfused transcardially with 1× PBS, followed by 4% PFA. Whole brains were isolated and further fixed with 4% PFA for 4–5 h. Brains were cryosectioned in 30%

sucrose (diluted in 1× PBS) and cut frozen coronally on a freezing sliding microtome at 40 µm. Brain sections were stained with DAPI for hippocampal measurements.

In situ hybridization. Section ISH was performed as previously described[9] using RNase-free reagents and solutions. Briefly, the brain tissue sections from matching littermate control and knock-in animals were mounted on a single slide and air dried. The sections were then rinsed in 1× PBS, steamed in 10 mM sodium citrate, pH 6, washed in 1× PBS and acetylated for 10 min (1.3% triethanolamine, 0.06% hydrogen chloride and 0.38% acetic anhydride). The sections were prehybridized for 1 h at 65 °C (in a solution of 50% formamide, 50 µg ml^{-1} of heparin, 50 µg ml^{-1} of yeast transfer RNA, 5× saline–sodium citrate (SSC) and 1% sodium dodecylsulfate), followed by hybridization with digoxigenin (DIG)-labeled riboprobe overnight at 65 °C. The VIP probe was designed against exons 2–6, linearized with HindIII and transcribed with a DIG-labeling mix using the T7 polymerase (Roche). The *Arx* probe was designed against exons 5 and 6 (chrX:9054137-90543401 in mm9), linearized with PstI, and transcribed with a DIG-labeling mix using the T7 polymerase (Roche). Probes were purified using an RNA clean and concentrator kit (Zymo Research). The next day, sections were first washed in 5× SSC, pH 4.5 for 5 min at room temperature, and then twice in 0.2× SSC at 72 °C for 30 min. After a 5-min wash in NTT (0.15 M sodium chloride, 0.1 M Tris, pH 8, 0.1% Tween), the sections were blocked in 5% heat-inactivated sheep serum in 2% blocking reagent in NTT for 1 h at room temperature. Sections were then incubated overnight in anti-DIG-AP antibody. The next day, after three washes in NTTML (0.15 M sodium chloride, 0.1 M Tris, pH 9.5, 0.1% Tween, 50 mM $MgCl_2$, 2 mM levamisole), the signal was revealed using BM purple at 37 °C overnight. Finally, the sections were coverslipped and imaged.

Brain section image acquisition and analysis. Brightfield images were acquired with a Coolsnap camera (Photometrics) mounted on a microscope (Nikon Eclipse 80i) using Nikon NIS Elements acquisition software, v.3.22.15 (Build 738). Image brightness and contrast were adjusted and images were merged using Adobe Photoshop.

Hippocampal measurements. Dentate gyrus length was measured using ImageJ software[37] by tracing the total lengths of the superior and inferior blades of the gyrus on serial sections of the left and right hippocampi after the appearance of the superior limb of the dentate gyrus. Measurements were taken blinded to each animal's genotype. Dentate gyrus lengths obtained from hs122 enhancer knock-in mice were normalized to wild-type littermate controls for reporting in Fig. 4. Raw measurements are reported in Supplementary Table 3 and plotted in Extended Data Fig. 9.

Cell counting. To assess VIP$^+$ cell density in the postnatal neocortex on brain sections, ×8 magnification brightfield images were taken of the somatosensory cortex at the level of the fornix. Images were opened in Adobe Photoshop and boxes of proportional dimensions encompassing all layers of the cortex were drawn for three serial sections from each animal. Images were then opened with ImageJ, and Cell Counter was used to count all cells within the determined box. Cell counts were divided by the area of the region of interest to determine cell density. Measurements were performed blinded to each animal's genotype. Cell density counts obtained for hs121 enhancer knock-in mice were normalized to wild-type littermates for reporting in Fig. 5. Raw measurements are reported in Supplementary Table 4 and plotted in Extended Data Fig. 10.

Motif enrichment analysis. First, the coordinates of 370 nonexonic ultraconserved sequences (type 'p' and 'n')[1] were lifted over[26] to hg19. HOMER[38] findMotifsGenome.pl script was used to find transcription factor motifs enriched in these sequences with the parameter '-size' given (Extended Data Fig. 4a). Next, the coordinates of 16-bp windows centered around the coordinates of mutations introduced into 23 ultraconserved enhancers in the present study were used in HOMER findMotifsGenome.pl script to determine the motifs enriched in sequences overlapping mutations (Extended Data Fig. 4b). Mutations were split into those that led to decrease/loss of enhancer activity and those that did not. Finally, to directly compare the mutations introduced into the same enhancer with different outcomes in enhancer activity, the bedtools (v.2.27.1) intersect was used to overlap JASPAR[39] transcription factor motifs (score ≥ 400) with mutations in eight enhancers that had mutant alleles with 5% of base pairs changed, for which one allele led to decrease/loss of this enhancer activity, whereas the other did not (Extended Data Fig. 4c).

Statistics and data processing. Statistical analyses and plot generation were done with R v.3.5.0 (www.r-project.org). For transgenic assay results to classify an enhancer allele as impacted by mutation, we determined whether differences in enhancer activity levels between reference and mutant alleles were statistically significant (two-tailed Fisher's exact test, $P < 0.05$). The test compared the number of embryos classified as strong, weak or absent for each allele. Number of embryos tested and *P* values from Fisher's exact tests are reported in Supplementary Tables 1 and 2. To determine statistical differences in hippocampal measurement for hs122 and cell counts for hs121 enhancer knock-in mouse lines, two-tailed Student's *t*-tests were performed between littermate controls paired by age/processing batch to account for potential differences in ISH. Characteristics of phenotyped mice and raw measurements are reported in Supplementary Tables 3 and 4 and plotted in Extended Data Figs. 9 and 10. Number of animals and *P* values are reported in legends of Figs. 5b and 6b.

Reporting Summary. Further information on research design is available in the Nature Research Reporting Summary linked to this article.

Data availability

Images of all transgenic whole-mount-stained embryos are included in Supplementary Fig. 1. Images of brains sections from knock-in animals and wild-type littermates are in Extended Data Figs. 8, 9 and 10. Human single-nucleotide variants were obtained from TOPMed (https://bravo.sph.umich.edu/freeze5/hg38) in June 2020. JASPAR transcription factor motif data were downloaded from http://expdata.cmmt.ubc.ca/JASPAR/downloads/UCSC_tracks/2018/hg19. Public chromatin immunoprecipitation sequencing data were obtained from https://www.encodeproject.org (mouse embryonic H3K27ac and H3K27me3, mouse and human CTCF) and https://www.ncbi.nlm.nih.gov/geo/query/acc.cgi?acc=GSE124936 (DLX transcription factors). The cloning vector for the transgenic assay (PCR4-Shh::lacZ-H11) is available from Addgene (catalog no. 139098). All other vectors described in the present study are available from the authors upon request. Transgenic embryos and stable knock-in lines can also be made available upon request.

References

33. Pollard, K. S., Hubisz, M. J., Rosenbloom, K. R. & Siepel, A. Detection of nonneutral substitution rates on mammalian phylogenies. *Genome Res.* **20**, 110–121 (2010).
34. Gibson, D. G. et al. Enzymatic assembly of DNA molecules up to several hundred kilobases. *Nat. Methods* **6**, 343–345 (2009).
35. Kvon, E. Z. et al. Progressive loss of function in a limb enhancer during snake evolution. *Cell* **167**, 633–642.e11 (2016).
36. Montague, T. G., Cruz, J. M., Gagnon, J. A., Church, G. M. & Valen, E. CHOPCHOP: a CRISPR/Cas9 and TALEN web tool for genome editing. *Nucleic Acids Res.* **42**, W401–W407 (2014).
37. Schneider, C. A., Rasband, W. S. & Eliceiri, K. W. NIH image to ImageJ: 25 years of image analysis. *Nat. Methods* **9**, 671–675 (2012).
38. Heinz, S. et al. Simple combinations of lineage-determining transcription factors prime *cis*-regulatory elements required for macrophage and B cell identities. *Mol. Cell* **38**, 576–589 (2010).
39. Khan, A. et al. JASPAR 2018: update of the open-access database of transcription factor binding profiles and its web framework. *Nucleic Acids Res.* **46**, D1284 (2018).

Acknowledgements

This work was supported by the US National Institutes of Health (grant no. R01HG003988 to L.A.P.), the National Institute of Neurological Disorders and Stroke (grant no. R01NS034661 to J.L.R.R.) and the National Institute of Mental Health (grant no. R01MH049428 to J.L.R.R.). A.R.Y. was supported by a grant from Fondation Fyssen. Research was conducted at the E.O. Lawrence Berkeley National Laboratory and performed under US Department of Energy contract DE-AC02-05CH11231, University of California. We thank F. Darbellay and S. Rajderkar for help with embryo scoring. We also thank J. Hu (UCSF) for kindly providing the VIP riboprobe.

Author contributions

V.S., A.R.Y., B.J.M., I.P.-F., C.S.N., A.N.H., Q.T.P., M.K., E.Z.K., Y.Z., M.S., R.D.H., E.M., J.G., J.A.A., S.T. and V.A. performed experiments, including making and/or characterizing all transgenic and knock-in mouse lines. V.S., D.E.D., A.V., L.A.P., A.R.Y. and J.L.R.R. planned the study and wrote the manuscript with input from the remaining authors.

Competing interests

J.L.R.R. is a cofounder and stockholder, and currently on the scientific board of Neurona, a company studying the potential therapeutic use of interneuron transplantation. The other authors declare no competing interests.

Additional information

Extended data is available for this paper at https://doi.org/10.1038/s41588-021-00812-3.

Supplementary information The online version contains supplementary material available at https://doi.org/10.1038/s41588-021-00812-3.

Correspondence and requests for materials should be addressed to A.V., L.A.P. or D.E.D.

Peer review information *Nature Genetics* thanks Menno Creyghton, Stephen Gisselbrecht, Katherine Pollard and the other, anonymous, reviewer(s) for their contribution to the peer review of this work.

Reprints and permissions information is available at www.nature.com/reprints.

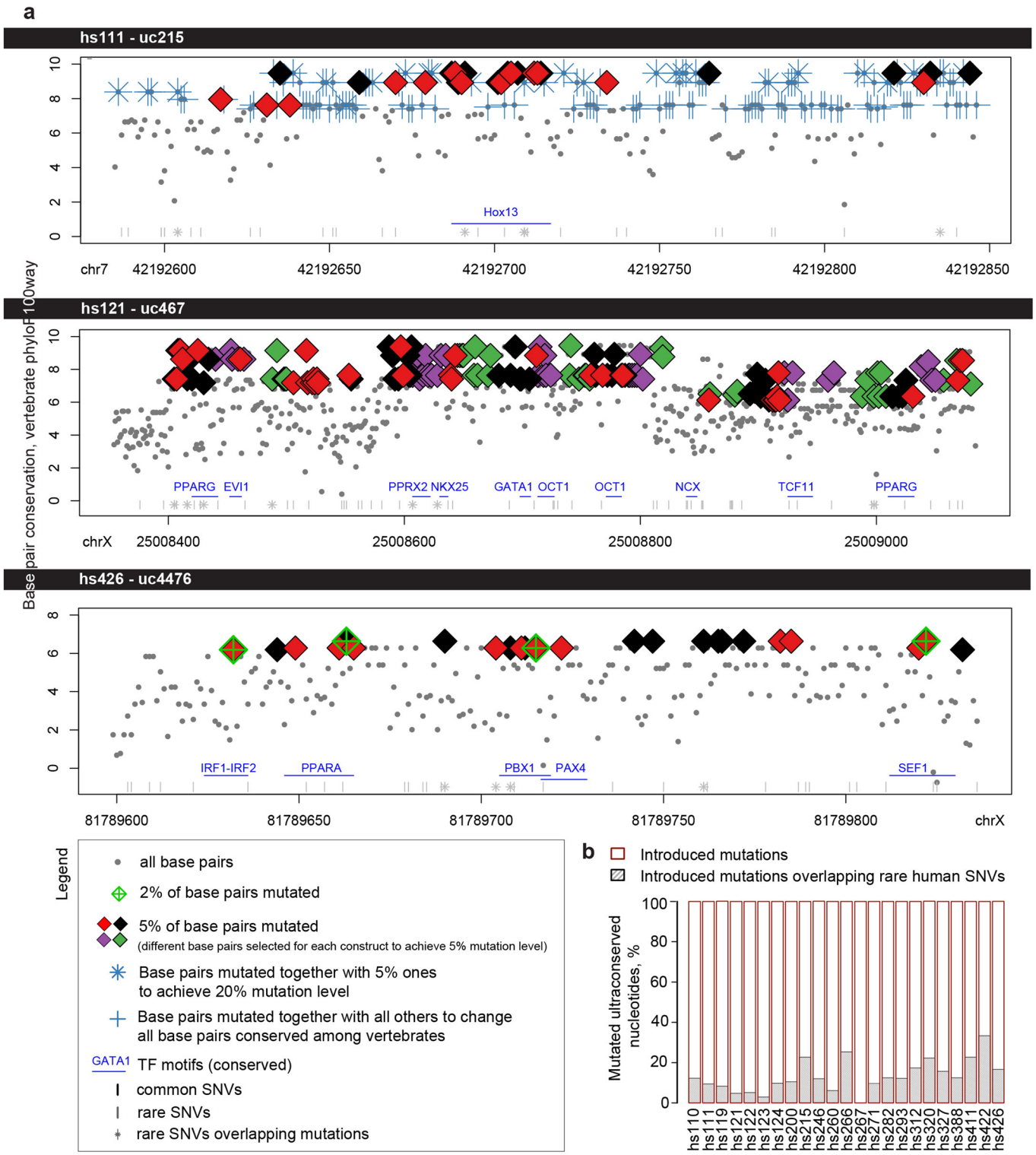

Extended Data Fig. 1 | Characterization of base pairs selected for mutagenesis. a, Detailed breakdown of conservation (phylop100way score) and position of base pair mutations for selected examples of ultraconserved enhancers mutated in this study. Base pairs selected to achieve various levels of mutagenesis: 2%, 5%, 20%, or all base pairs conserved among ~100 vertebrates are marked according to the legend. All coordinates are in hg19. Locations of conserved transcription factor motifs[26] and human SNVs (TOPMed, https://bravo.sph.umich.edu/freeze5/hg38/) are also included (see legend). See Supplementary Information for similar plots of all 23 ultraconserved enhancers selected for mutagenesis. **b**, Percentage of mutations introduced into ultraconserved sequences that also overlapped human SNVs (all overlap rare human variants, that is found in <1% of human population. No introduced mutations overlap a SNV common in the human population).

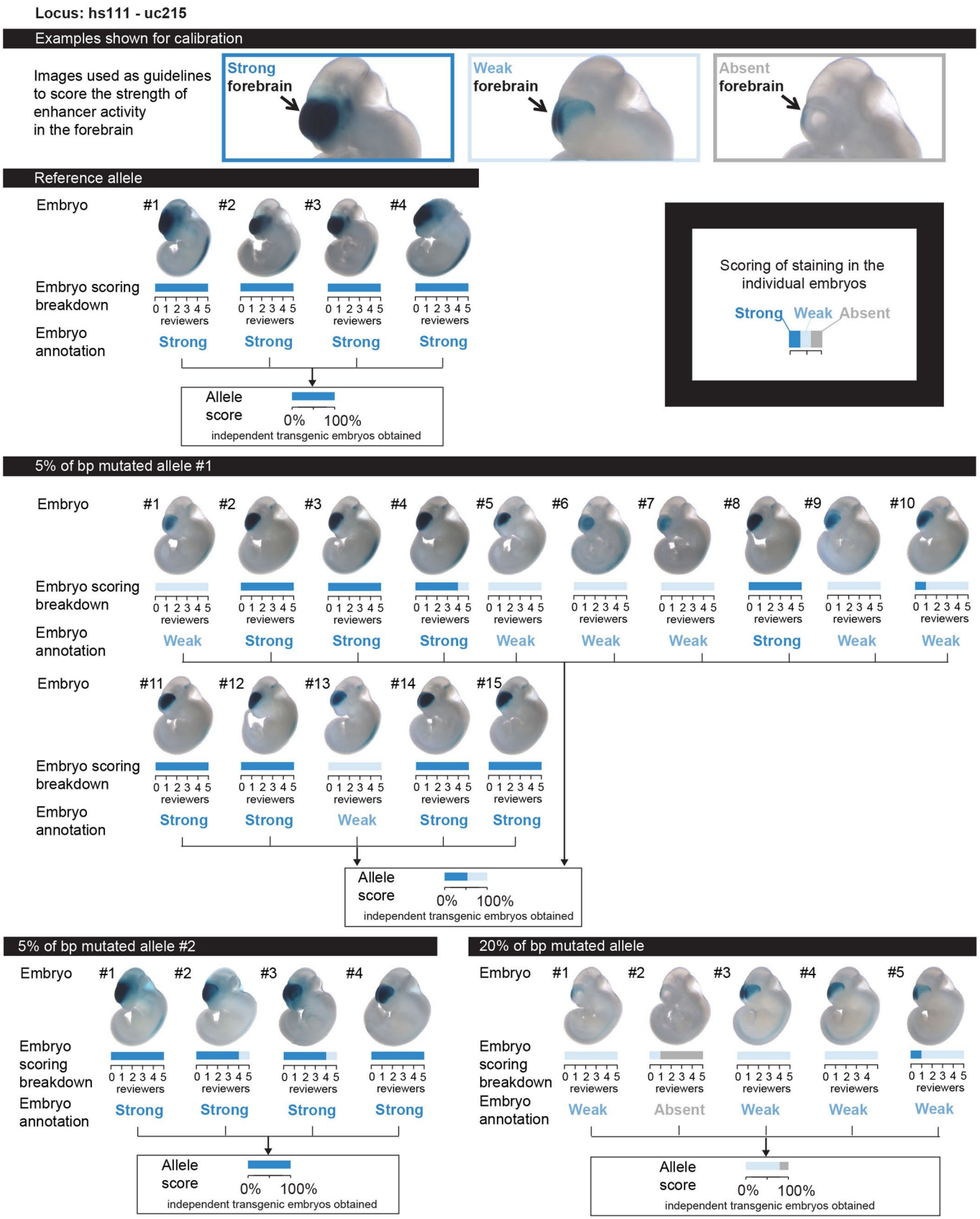

Extended Data Fig. 2 | See next page for caption.

Extended Data Fig. 2 | Example of enhancer scoring. Top: calibration images given for one ultraconserved enhancer (hs111) to show different categories of enhancer activity. Randomized embryo images were shown to five reviewers alongside the calibration images displayed at the top. The reviewers scored the strength of enhancer activity independently and blind to the identity of the enhancer allele. Bottom: breakdown of enhancer activity scoring results per embryo for four different alleles tested for the hs111 enhancer: reference allele, allele with 5% of bp mutated #1, allele with 5% of bp mutated #2, and allele with 20% of bp mutated. See Supplementary Information for a similar scoring breakdown of all 23 ultraconserved enhancers selected for mutagenesis.

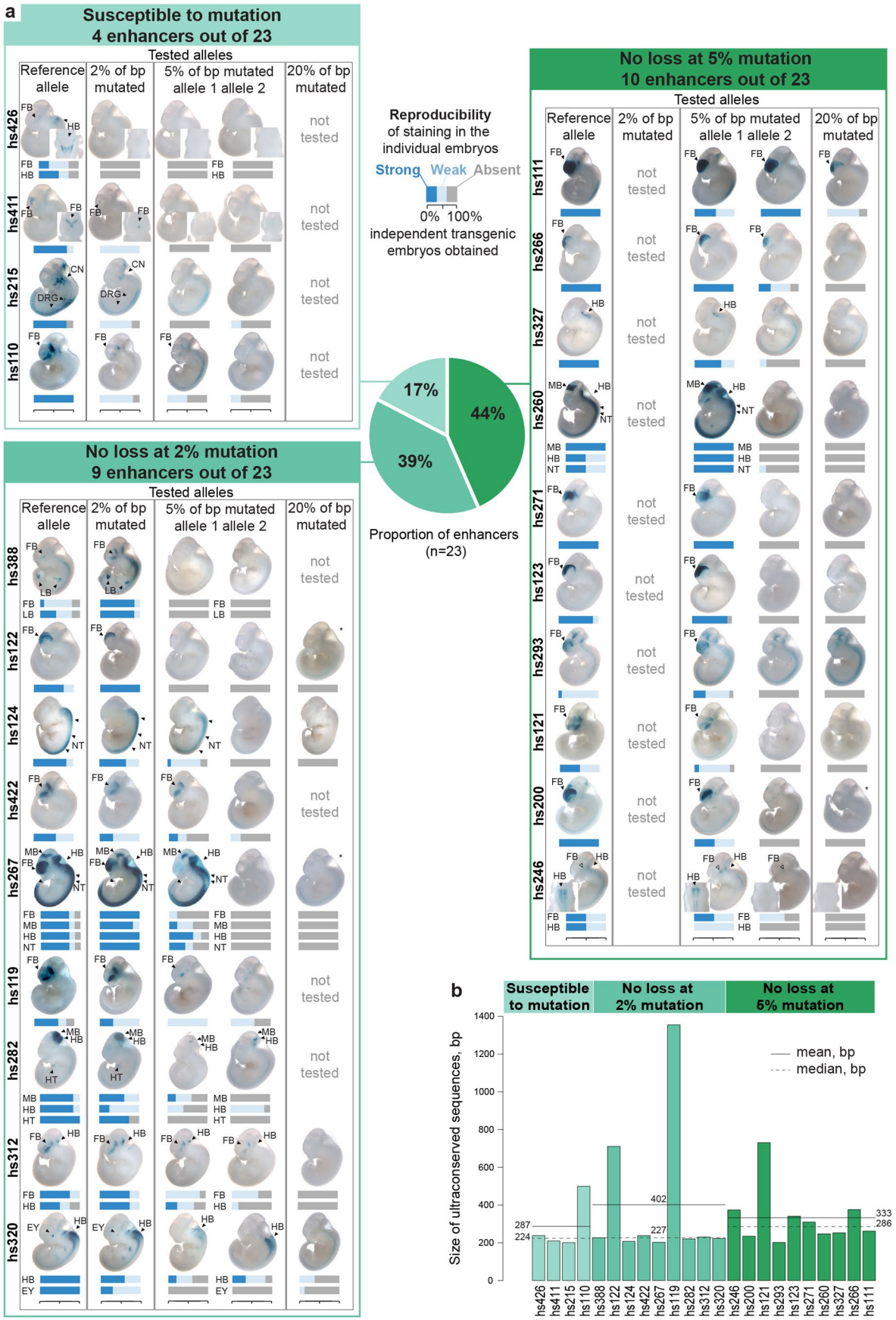

Extended Data Fig. 3 | See next page for caption.

Extended Data Fig. 3 | Distribution of 23 ultraconserved enhancers among the three groups of enhancer mutagenesis outcomes. a, Images of embryos and enhancer activity results for all 23 enhancers. Bar plots under the embryo images show the strength and reproducibility of LacZ staining (serving as a proxy for enhancer activity) among individual transgenic embryos from each enhancer allele. Enhancer activity was scored by five independent reviewers blind to the embryo genotype after the images were randomized (see Methods, Extended Data Fig. 2 and Supplementary Information for details). Embryo images for CRISPR-assisted transgenic experiments for the reference alleles of enhancers hs200 and hs215 were published previously[24]. All other transgenic assays were newly performed for this study. All of the mutation alleles tested harbored sequence changes at 2, 5, or 20% of ultraconserved bases, as indicated above, with the exception of three of the alleles grouped with the 20% variants (marked with an asterisk [*] for hs122, hs200, and hs267). For the hs122 allele, 25% of bp were actually mutated. For hs200 (16% mutation) and hs267 (12% mutation), fewer than 20% of base pairs are well-conserved among ~100 vertebrates, so lower levels of mutagenesis were used. CN, cranial nerve; DRG, dorsal root ganglia; EY, eye; FB, forebrain; HB, hindbrain; HT, heart; LB, limb; MB, midbrain; NT, neural tube. **b**, Length of ultraconserved sequences for all 23 enhancers arranged by enhancer mutagenesis outcomes with mean and median shown per group as solid and dashed lines, respectively. No statistically significant differences detected between groups (two-tailed t-tests). bp, base pairs.

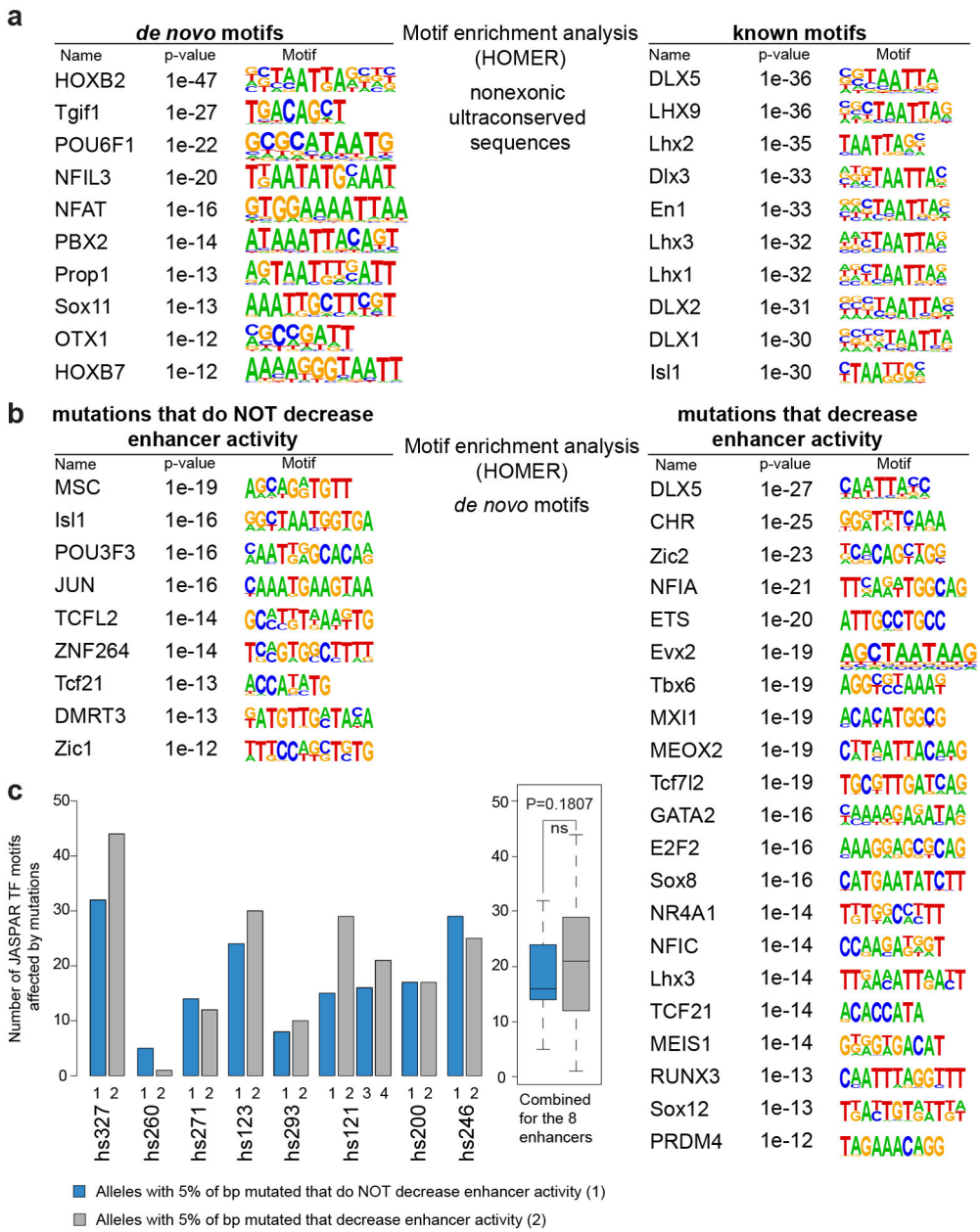

Extended Data Fig. 4 | See next page for caption.

Extended Data Fig. 4 | Motif enrichment analysis. a, Motifs that are significantly enriched in 370 noncoding ultraconserved sequences compared to the whole human genome. **b**, Motifs that are significantly enriched in 15 base pair k-mers centered on introduced mutations compared to the whole human genome. **c**, Left: Bar plot comparing the number of transcription factor motifs in the JASPAR database that overlap introduced mutations in alleles of the same enhancer that either decreased enhancer activity (grey bars) or not (blue bars). Each allele has 5% of ultraconserved base pairs mutated. Right: Boxplot summarizing data from all eight enhancers shown in the bar plot. Data is presented as median in the center, first (25^{th} percentile) and third (75^{th} percentile) quartile as bounds of the boxes, and $\pm$ 1.5 x ICR (interquartile range = third – first quartile) from bounds of the boxes as whiskers. **d**, Left: Bar plot showing the percentage of JASPAR transcription factor motifs overlapping 23 enhancers mutated in this study that occur in the ultraconserved sequence of an enhancer only once (unique, black) or multiple times (redundant, grey). On average, 48% of motifs were unique. Right: Bar plot comparing distribution of unique vs. redundant transcription factor motifs that overlap introduced mutations between mutant alleles that resulted in decreased enhancer activity (grey bars) and those that did not (blue bars). On average, ~52% of motifs that overlapped introduced mutations that did not decrease enhancer activity were unique, while the average for unique motifs that overlapped introduced mutations that decreased enhancer activity was ~44%.

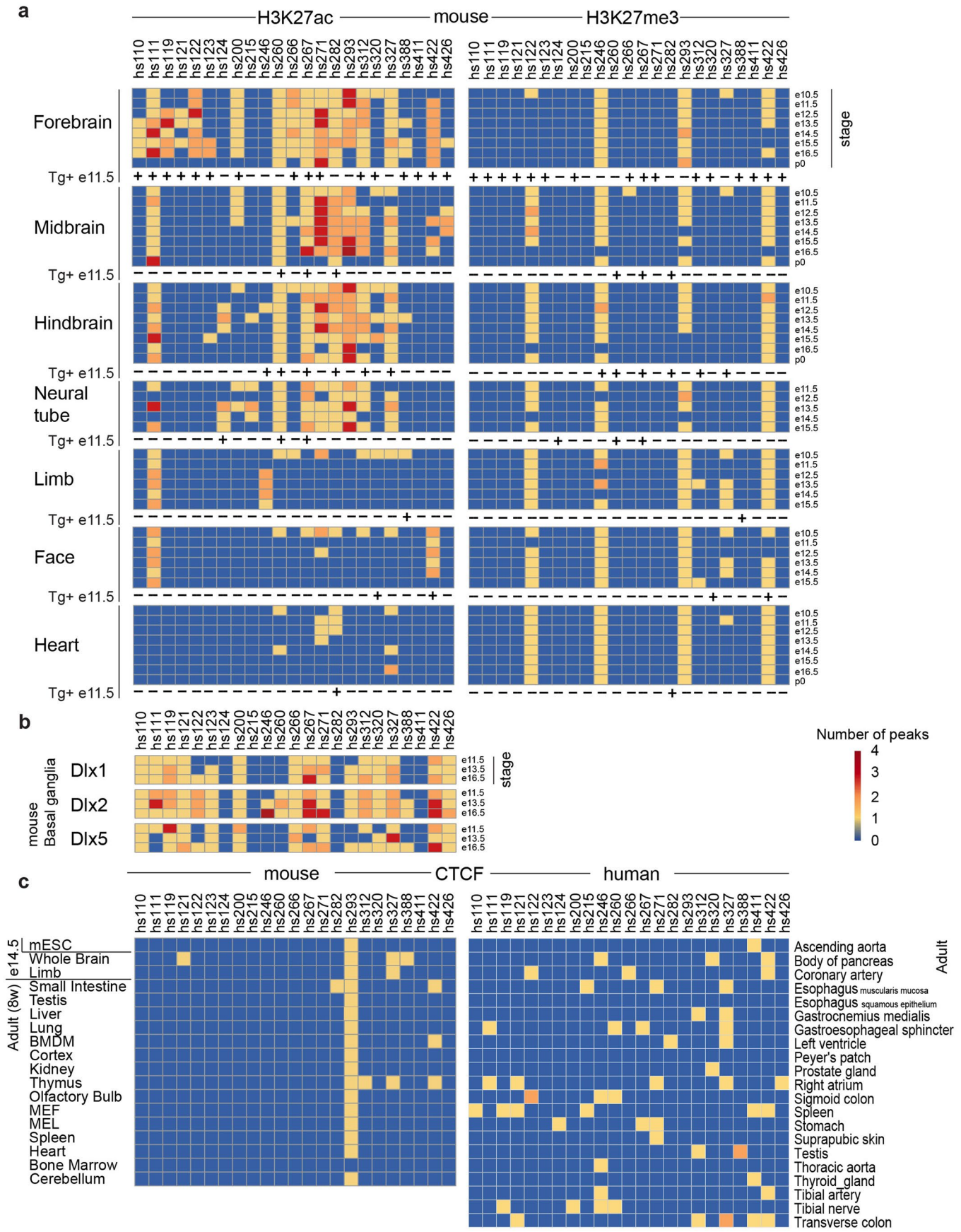

Extended Data Fig. 5 | See next page for caption.

Extended Data Fig. 5 | Chromatin signatures of 23 ultraconserved enhancers mutated in this study in multiple tissues and developmental times points in mouse and human. a, Histone modifications associated with active enhancers (H3K27ac) and inactive sequences (H3K27me3) sampled from multiple tissues throughout mouse development. '+' and '-' for 'Tg+ e11.5' indicate the presence or absence, respectively, of the activity by the reference enhancer allele in e11.5 (e12.5 for hs124) transgenic mouse embryos reported in this study. ChIP-seq data was obtained from Gorkin *et al*., 2020[40]. **b**, Binding of Dlx transcription factors during embryonic development of mouse basal ganglia. ChIP-seq data was obtained from Lindtner *et al*., 2019[41]. **c**, Binding of CTCF in embryonic and adult mouse tissues and adult human tissues. ChIP-seq data was obtained from Yue *et al*., 2014[42] for mouse samples and from Dunham *et al*., 2012[43] for human samples.

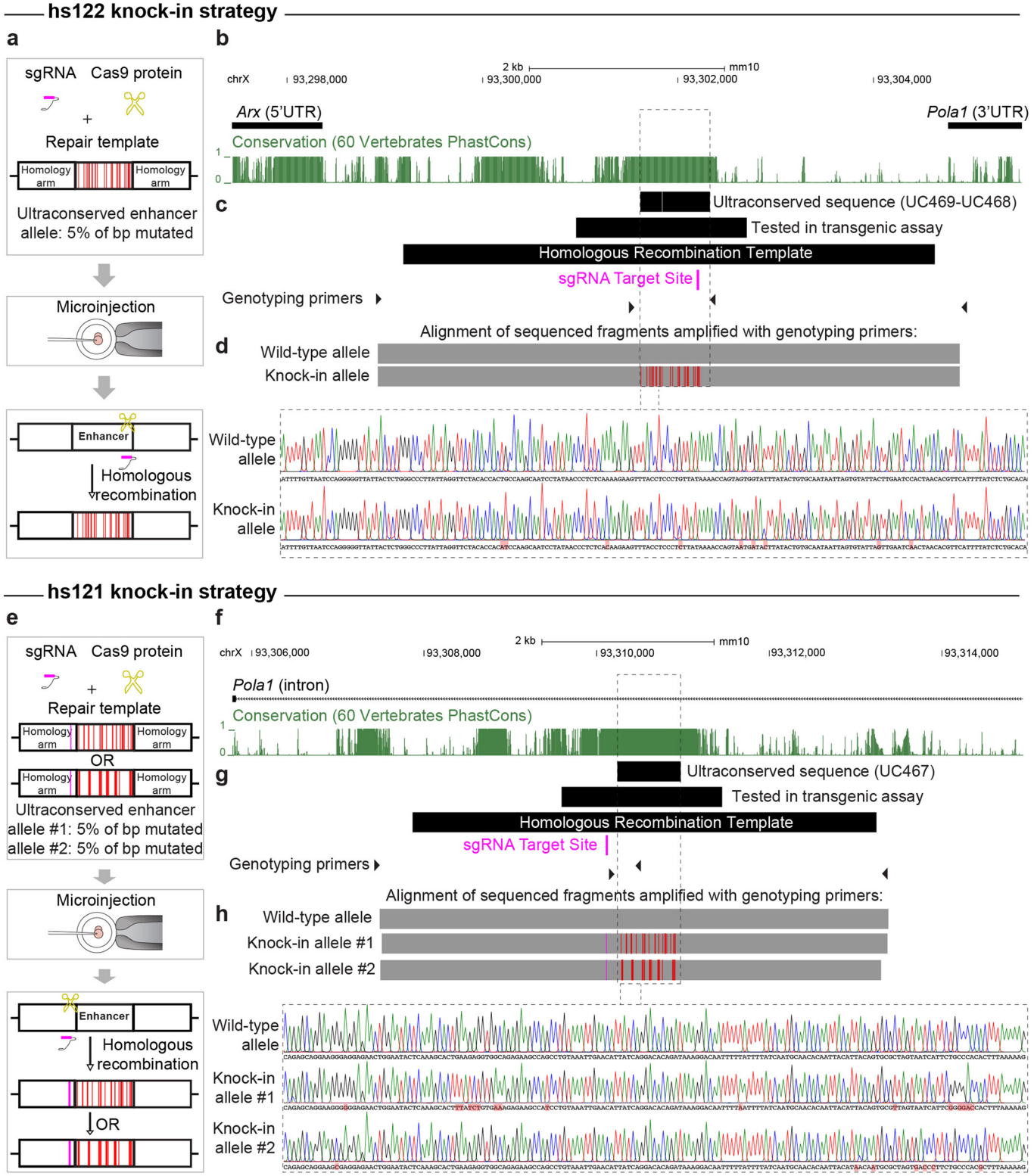

Extended Data Fig. 6 | See next page for caption.

Extended Data Fig. 6 | Knock-in strategy to introduce the mutations into the endogenous mouse alleles of hs122 (uc468+uc469) and hs121 (uc467). **a, e**, The mutant enhancer alleles were knocked-in via homologous recombination of the reference allele via a CRISPR/Cas9 microinjection protocol. A sgRNA for hs122 was designed to target the reference allele sequence that overlaps mutations introduced into the mutant allele. The target sequence of a sgRNA for hs121 was 115 bp upstream of the ultraconserved sequence, thus hs121 repair templates carried a point mutation altering the PAM sequence for the sgRNA (schematically indicated by the pink lines) to prevent their cleavage by the CRISPR/Cas9 complex. **b, f**, The genomic region between the *Arx* and *Pola1* genes contains hs122, and hs121 is located in the first intron of the *Pola1* gene. Conservation tracks (green) show phastCons scores between mouse and other vertebrate genomes. **c, g**, Positions of the ultraconserved sequences within enhancers (uc468+uc469 OR uc467), the sequences tested in the transgenic assay, the homologous recombination templates, and genotyping primers are shown schematically in black. Position of the sgRNA target sites shown in pink. **d, h**, Males hemizygous for the mutant alleles of the hs122 and hs121 enhancers were genotyped with PCR amplification (positions of genotyping primers shown as black triangles in **c** and **g**) and Sanger sequencing. Top: alignment of reads from the knock-in alleles and wild-type alleles to the reference mouse genome (mm10) is shown in grey, with mismatches indicating the location of the introduced mutations represented by red lines. Bottom: Sanger sequencing traces for mutant knock-in and wild-type alleles are shown for the region within the dotted lines. Introduced mutations are highlighted in red. See Supplementary Tables 4, 5 for more information on coordinates and sequences.

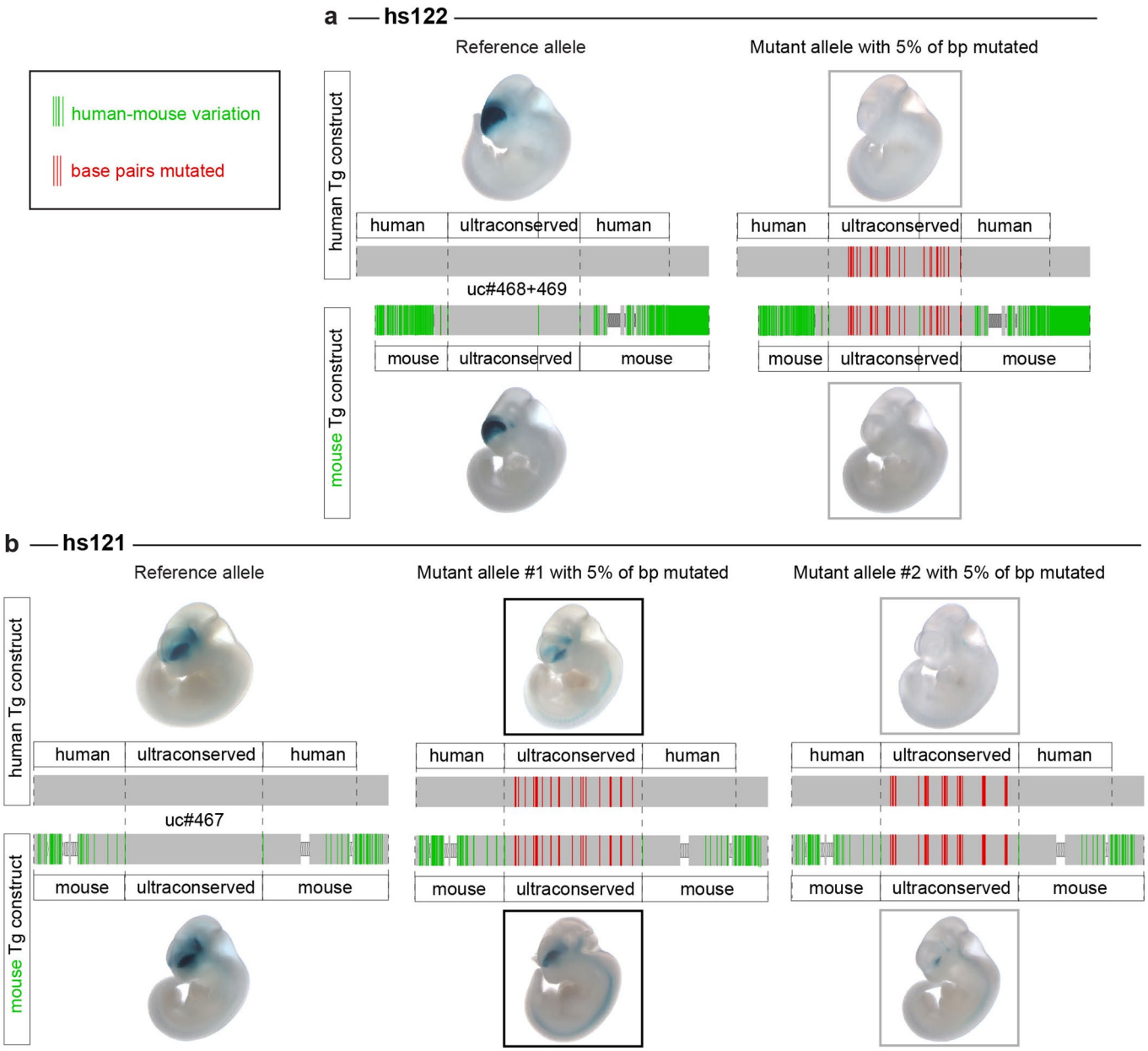

Extended Data Fig. 7 | Transgenic reporter assays with either human or mouse sequences surrounding the ultraconserved core show the same effect on the enhancer activity. The sequences surrounding the ultraconserved parts of the (**a**) hs122 (uc468+uc469) and (**b**) hs121 (uc467) enhancers tested in transgenic assays differ between the human and mouse genomes (mismatches shown in green). To make sure that mouse regions flanking the ultraconserved sequences (shown in red) will not compensate for mutations introduced into the endogenous mouse alleles of the enhancers, we tested the activity of the mouse sequence in transgenic assays for both the reference alleles and the alleles with 5% of base pairs mutated. Regions to test were selected to span the hs122 and hs121 sequences deleted from the mouse genome previously[9].

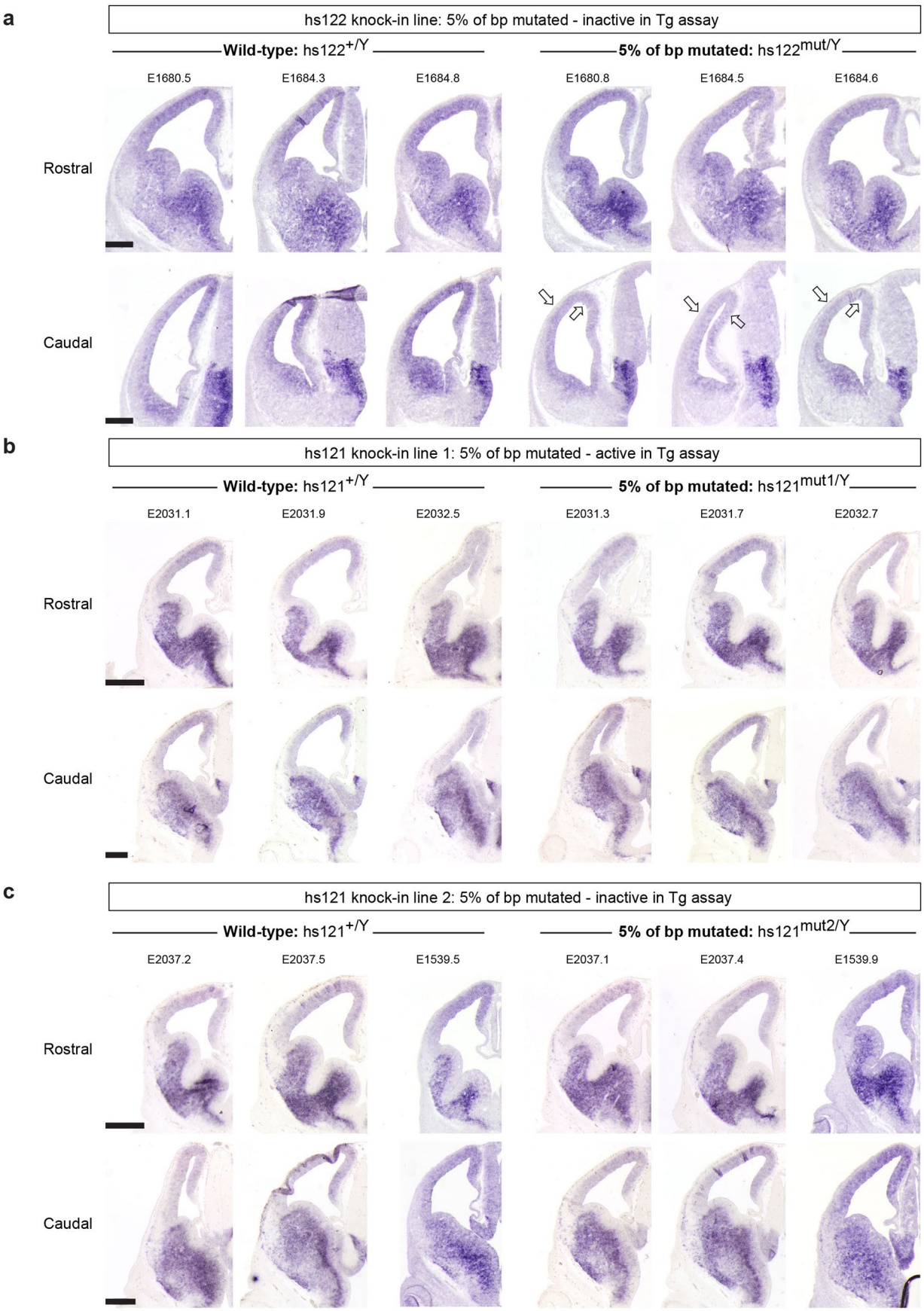

Extended Data Fig. 8 | See next page for caption.

Extended Data Fig. 8 | *Arx* expression in mice with mutated endogenous hs121 and hs122 enhancers. *In situ* hybridization for *Arx* expression (purple staining) performed on coronal cross-sections of e12.5 forebrains from hemizygous knock-in males shown alongside wild-type littermate controls from three knock-in lines: (**a**) hs122^{mut} (allele with 5% of base pairs mutated that eliminated enhancer activity in mouse transgenic assay), (**b**) hs121^{mut1} (allele with 5% of base pairs mutated that did not affect enhancer activity in mouse transgenic assay), and (**c**) hs121^{mut2} (allele with 5% of base pairs mutated that eliminated enhancer activity in mouse transgenic assay). Arrows point to a loss of *Arx* signal in the caudal cortical regions of hs122$^{mut/Y}$ sections. We did not detect changes in *Arx* expression in hemizygous knock-in male embryos for either of the hs121 enhancer mutant alleles (hs121$^{mut1/Y}$ and hs121$^{mut2/Y}$). However, this is consistent with the data from hs121-null embryos[9], and is likely due to tissue heterogeneity and the presence of another *Arx* enhancer (hs119) with a similar activity domain. Scale bars, 200 μm.

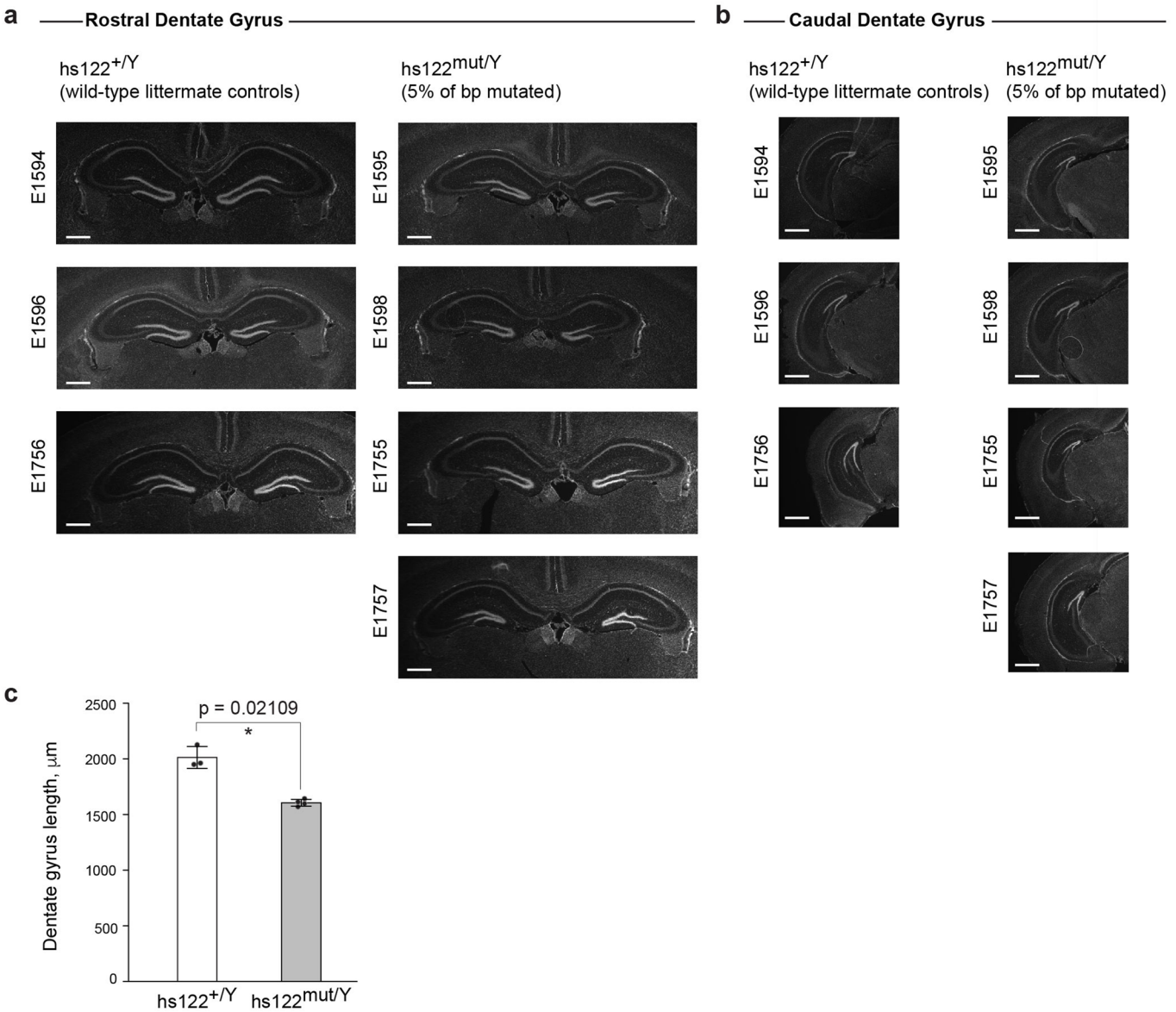

Extended Data Fig. 9 | Mutagenesis of the endogenous hs122 enhancer results in dentate gyrus abnormalities (a smaller dentate gyrus with disorganized appearance). Rostral (**a**) and caudal (**b**) coronal cross-sections of postnatal hippocampus from all phenotyped animals: three wild-type littermate male controls and four hemizygous knock-in males shown side-by-side for comparison. Numbers represent unique identifiers for each mouse examined (details in Supplementary Table 6). Scale bars, 500 µm. **c**, Bar graph showing quantification of dentate gyrus length for wild-type mice (n = 3) and knock-in mice (n = 4). Bars indicate mean lengths, with individual biological replicates represented by dots. Error bars, mean ± s.d. Difference in length between wild-type and knock-in mice assessed by a two-tailed paired t-test.

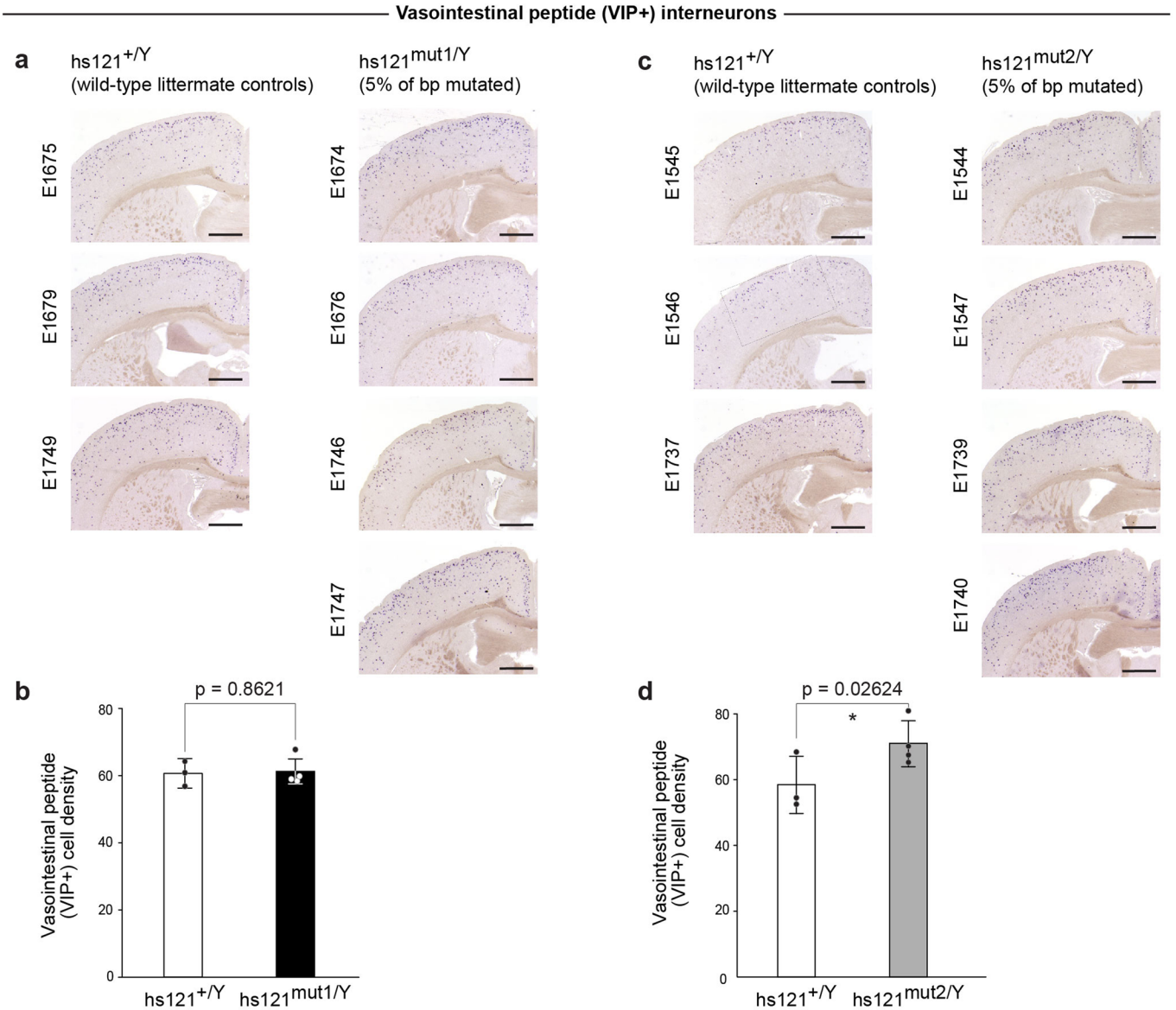

Extended Data Fig. 10 | Mutagenesis of the endogenous hs121 enhancer results in abnormalities in the number of vasointestinal peptide (VIP+) interneurons in adult mice brains only for the allele that abolished hs121 enhancer activity in transgenic reporter assay. Coronal cross-sections through cortex from two knock-in lines generated for mutant alleles of the hs121 enhancer: one that was active (**a**) in the transgenic reporter assay and one that was inactive (**c**). Representative images shown from all phenotyped animals: three wild-type littermate male controls and four hemizygous knock-in males for each allele, displayed side-by-side for comparison. Numbers represent unique identifiers for each mouse examined (details in Supplementary Table 7). Scale bars, 1 mm. **b, d**, Bar graphs showing quantification of VIP+ interneuron densities (cells/mm^2) between wild-type (n = 3) and knock-in (n = 4) mice. Bars indicate mean densities, with individual biological replicates represented by dots. Error bars, mean ± s.d. Differences between wild-type and knock-in mice assessed by two-tailed paired t-tests.

nature research

Corresponding author(s): Axel Visel, Len Pennacchio, Diane Dickel

Last updated by author(s): 1/28/2021

Reporting Summary

Nature Research wishes to improve the reproducibility of the work that we publish. This form provides structure for consistency and transparency in reporting. For further information on Nature Research policies, see Authors & Referees and the Editorial Policy Checklist.

Statistics

For all statistical analyses, confirm that the following items are present in the figure legend, table legend, main text, or Methods section.

n/a	Confirmed	
☐	☒	The exact sample size (*n*) for each experimental group/condition, given as a discrete number and unit of measurement
☒	☐	A statement on whether measurements were taken from distinct samples or whether the same sample was measured repeatedly
☐	☒	The statistical test(s) used AND whether they are one- or two-sided *Only common tests should be described solely by name; describe more complex techniques in the Methods section.*
☒	☐	A description of all covariates tested
☒	☐	A description of any assumptions or corrections, such as tests of normality and adjustment for multiple comparisons
☒	☐	A full description of the statistical parameters including central tendency (e.g. means) or other basic estimates (e.g. regression coefficient) AND variation (e.g. standard deviation) or associated estimates of uncertainty (e.g. confidence intervals)
☐	☒	For null hypothesis testing, the test statistic (e.g. *F*, *t*, *r*) with confidence intervals, effect sizes, degrees of freedom and *P* value noted *Give P values as exact values whenever suitable.*
☒	☐	For Bayesian analysis, information on the choice of priors and Markov chain Monte Carlo settings
☒	☐	For hierarchical and complex designs, identification of the appropriate level for tests and full reporting of outcomes
☒	☐	Estimates of effect sizes (e.g. Cohen's *d*, Pearson's *r*), indicating how they were calculated

Our web collection on statistics for biologists contains articles on many of the points above.

Software and code

Policy information about availability of computer code

Data collection	Transgenic embryos were imaged with Adobe Photoshop Elements 11. Brain sections were imaged with Nikon NIS Elements acquisition software, version 3.22.15 (Build 738).
Data analysis	Statistical analyses and plot generation were done with R version 3.5.0 (www.r-project.org).

For manuscripts utilizing custom algorithms or software that are central to the research but not yet described in published literature, software must be made available to editors/reviewers. We strongly encourage code deposition in a community repository (e.g. GitHub). See the Nature Research guidelines for submitting code & software for further information.

Data

Policy information about availability of data

All manuscripts must include a data availability statement. This statement should provide the following information, where applicable:

- Accession codes, unique identifiers, or web links for publicly available datasets
- A list of figures that have associated raw data
- A description of any restrictions on data availability

Images of all transgenic whole-mount-stained embryos are included in Supplementary Figure 1. Images of brains sections from knock-in animals and wild-type littermates are in Extended Data Fig. 8, 9, and 10. Human SNVs were obtained from TOPMed, https://bravo.sph.umich.edu/freeze5/hg38/ in June 2020. JASPAR transcription factor motif data was downloaded from http://expdata.cmmt.ubc.ca/JASPAR/downloads/UCSC_tracks/2018/hg19/. Public ChIP-seq data was obtained from https://www.encodeproject.org (mouse embryonic H3K27ac and H3K27me3, mouse and human CTCF) and https://www.ncbi.nlm.nih.gov/geo/query/acc.cgi?acc=GSE124936 (Dlx transcription factors).

Field-specific reporting

Please select the one below that is the best fit for your research. If you are not sure, read the appropriate sections before making your selection.

☒ Life sciences ☐ Behavioural & social sciences ☐ Ecological, evolutionary & environmental sciences

For a reference copy of the document with all sections, see nature.com/documents/nr-reporting-summary-flat.pdf

Life sciences study design

All studies must disclose on these points even when the disclosure is negative.

Sample size	The transgenic embryo sample sizes were determined empirically based on our experience performing >4,000 transgenic enhancer assays (VISTA Enhancer Browser: https://enhancer.lbl.gov/). Activities of reference enhancer alleles were already known from random transgenic assays. For direct comparison to mutant enhancer alleles, we tested all reference alleles anew with targeted transgene assays and made sure to obtain at least two transgenic embryos positive for integration of a transgene into H11 locus, which enhancer activity patterns recapitulated those observed with random transgenic assays. For mutant enhancer alleles we required reproducible patterns to be present in at least three transgenic embryos positive for H11 integration. Number of embryos assayed for each allele are reported in Table S1.
Data exclusions	The embryos genotyped negative for transgene integration into the H11 locus were excluded from further analysis, along with embryos that were not at the correct developmental stage, were heavily damaged during collection or appeared developmentally abnormal.
Replication	In vivo transgenic mouse assays: across all 121 H11 transgenic experiments (distinct allele and developmental stage combinations) reported in the manuscript, ~60% were performed at least twice with the same results observed and for these, data across multiple litters was integrated. The rest of transgenic experiments were performed independently. For 4 enhancers (hs121, hs122, hs123, hs124) effects of mutagenesis was also tested using transgenic mice with random integration and the same results as with the targeted transgenene integration into H11 locus were observed (data not reported). Knock-in lines: for each line, neurological phenotyping was performed on 2 mouse litters with the same results observed.
Randomization	Images of transgenic embryos for each enhancer were pooled together for all alleles of that enhancer and randomized. Enhancer activity patterns for were scored by five independent reviewers blinded to the identity of enhancer allele. The process is described in details in Methods under section: Scoring the Strength of Ultraconserved Enhancer Activity in Transgenic Embryos. For neurological phenotyping wild-type and knock-in littermates were randomized and identified only by numbers with genotype unknown to the investigator during data collection, sample processing and measurement taking.
Blinding	For blinding in scoring of enhancer activity in transgenic embryos, see Randomization. Investigators were blinded to animals' genotype during data collection and measurements for neurological phenotyping of the three knock-in lines generated in this study.

Reporting for specific materials, systems and methods

We require information from authors about some types of materials, experimental systems and methods used in many studies. Here, indicate whether each material, system or method listed is relevant to your study. If you are not sure if a list item applies to your research, read the appropriate section before selecting a response.

Materials & experimental systems

n/a	Involved in the study
☒	☐ Antibodies
☒	☐ Eukaryotic cell lines
☒	☐ Palaeontology
☐	☒ Animals and other organisms
☒	☐ Human research participants
☒	☐ Clinical data

Methods

n/a	Involved in the study
☒	☐ ChIP-seq
☒	☐ Flow cytometry
☒	☐ MRI-based neuroimaging

Animals and other organisms

Policy information about studies involving animals; ARRIVE guidelines recommended for reporting animal research

Laboratory animals	All animal work done in this study was reviewed and approved by the Lawrence Berkeley National Laboratory Animal Welfare and Research Committee. Mice were housed in the animal facility, where their conditions were electronically monitored 24/7 with daily visual checks by technicians. Facility was also equipped with automatic alarms. Mice were housed in BioBubble Clean Rooms, soft-walled enclosures powered by 80-100 air changes per hour of HEPA filtration under Light/Dark Cycle of 12:12 starting at 6am, at 22-24.4C, and humidity 30-70%. All animals used in this study were of Mus musculus species and FVB strain. Sex was not determined for transgenic embryos, but cohorts are presumed to include roughly equal numbers of males and females. Transgenic embryos were assayed either at embryonic day 11.5 or 12.5 or 14.5.

	Phenotyping of mice in stable knock-in lines was done for males only due to studied enhancers located on chromosome X. Males were assayed at various ages ranging from postnatal day 32 to 67. Details are in Tables S6 and S7.
Wild animals	The study did not involve wild animals.
Field-collected samples	The study did not involve samples collected from the field.
Ethics oversight	All animal work done in this study was reviewed and approved by the Lawrence Berkeley National Laboratory Animal Welfare and Research Committee.

Note that full information on the approval of the study protocol must also be provided in the manuscript.